

# Optical probe of microwave current distributions in high temperature superconducting transmission lines

James C. Culbertson<sup>a)</sup> and Harvey S. Newman  
*Naval Research Laboratory, Washington, DC 20375-5347*

Charles Wilker  
*DuPont Superconductivity, Experimental Station, E304C120, Wilmington, Delaware 19880-0304*

(Received 23 July 1997; accepted for publication 27 April 1998)

This work develops two techniques for optically probing the spatial profile of microwave frequency superconducting currents. As an application, we measured the effects of high microwave powers on the spatial distribution of current on coplanar superconducting transmission lines fabricated using  $\text{YBa}_2\text{Cu}_3\text{O}_{7-\delta}$  and  $\text{Tl}_2\text{Ba}_2\text{CaCu}_2\text{O}_8$ . For both techniques, a focused light-spot served as the spatial probe whose effect was measured through the change in transmitted microwave power. For resonant geometries, the change was due to the kinetic-inductance bolometric effect; for nonresonant geometries, the change was due to the resistive-transition bolometric effect. Kinetic-inductance photoresponse measurements were acquired by setting the microwave frequency on the shoulder of a resonance and measuring the change in the microwave power transmitted through the device that occurred when the absorption of light shifted the frequency of the resonance. These kinetic-inductance measurements were performed as a function of microwave power on a  $\text{YBa}_2\text{Cu}_3\text{O}_{7-\delta}$  coplanar device at 74 K and on a  $\text{Tl}_2\text{Ba}_2\text{CaCu}_2\text{O}_8$  coplanar device at 80 K. Because the photoresponse in this technique is proportional to the *square* of the local current density underneath the light spot (as opposed to directly proportional), this technique is sensitive to current redistribution on length scales much smaller than the  $\sim 6 \mu\text{m}$  spatial resolution of our measurements. *Extrinsic* (defect and grain boundary associated) and *intrinsic* photoresponses were measured. Both coplanar samples showed no change in the intrinsic spatial distribution of the current as the microwave power was varied. At all temperatures the  $\text{Tl}_2\text{Ba}_2\text{CaCu}_2\text{O}_8$  sample exhibited substantial extrinsic spatial variations on a distance scale equal to the film's  $\sim 5 \mu\text{m}$  grain size; these spatial variations became more dramatic as the temperature  $T$  approached the critical temperature  $T_c$ . The spatial variations for the finer-grained  $\text{YBa}_2\text{Cu}_3\text{O}_7$  sample were much less pronounced. Behavior consistent with  $T_c$  being several degrees lower at the film edges was observed as  $T$  approached  $T_c$ ; the edge-current photoresponse started to narrow, increase faster than linearly with light power, and move away from the film edges toward the center of the strip; lowering the light power lessened these effects. Resistive-bolometric photoresponse measurements performed at temperatures within the resistive transition exhibited the same light power effects near  $T_c$ . The kinetic-inductance photoresponse can also be used as a probe of the local quality of unpatterned superconducting films; for this usage an unpatterned film serves as one wall of a resonant cavity and a focused light beam is scanned through the transparent substrate onto the underside of the superconducting film while monitoring the shift in the cavity resonance. © 1998 American Institute of Physics. [S0021-8979(98)03815-8]

## I. INTRODUCTION

In this work, we develop several techniques in which a focused light beam is used as a spatial probe of the current density in a superconductor. We then apply one of these techniques to study the possible redistribution of microwave frequency current in the limit of high current densities. The spatial distribution of currents and fields in high temperature superconductors at high microwave powers is an active area of interest for both theoretical and practical reasons.<sup>1-4</sup> There are significant advantages to using planar transmission line geometries in real applications. In planar geometries, superconducting thin films patterned in rectangular strips carry

current. It is at the edges of these strips (where the magnetic fields and the currents that screen them are the largest) that deviations from the low field and current behavior will first be encountered. In practical terms, this behavior can take the form of increased resistive loss and the increased generation of power in higher harmonics of the applied electromagnetic wave. It has been observed that when high microwave powers are applied to superconducting transmission lines, odd, harmonics of the applied frequency are generated.<sup>5</sup> In materials such as  $\text{YBa}_2\text{Cu}_3\text{O}_{7-\delta}$  (YBCO), the power generated in the third harmonic is proportional to the cube of the applied power (e.g.,  $P_3 = P_1^3$ ). In  $\text{Tl}_2\text{Ba}_2\text{CaCu}_2\text{O}_8$  (TBCCO), for a range of applied powers, the third harmonic increases much more slowly<sup>5</sup>—a desirable behavior. One model proposed to

<sup>a)</sup>Electronic mail: james.culbertson@nrl.navy.mil

explain the weaker harmonic generation in TBCCO at high microwave powers invokes the spatial redistribution of current in the superconducting film.<sup>5</sup>

In this work, we have used our kinetic-inductance photoresponse technique<sup>6</sup> and our new resistive-transition photoresponse technique to measure the spatial profile of microwave frequency current in superconductors and to study the spatial redistribution of current. In these techniques, a light spot focused on the superconducting film acts as the spatial probe. For kinetic-inductance measurements, as performed in this work, the superconducting region being probed must be part of a resonant transmission line structure. A kinetic-inductance photoresponse is acquired by setting the microwave frequency to be on the shoulder of a resonance and measuring the change in microwave transmission that occurs as the absorption of light heats up the film and shifts the frequency of the resonance. Using the kinetic-inductance photoresponse technique, spatial profiles of the current can be measured from temperatures near to well below the critical temperature  $T_c$  of the superconductor, whereas using the resistive-transition photoresponse technique measurements can be made only at temperatures within the resistive transition. These techniques have a theoretical spatial resolution on the order of the wavelength of the probing light in the region just above the superconducting film.

Our techniques have the advantage of high spatial resolution, fast response, and the lack of a physical probe in close proximity to the surface being probed (which could potentially perturb the field geometry). The possession of these three features is in distinct contrast with other reported spatial probes [e.g., superconducting quantum interference devices (SQUIDs),<sup>7–10</sup> Hall probes,<sup>11,12</sup> coaxial probes,<sup>13</sup> or field sensitive films placed in close proximity to the superconducting surface being studied<sup>14</sup>].

## II. THEORY BEHIND THE MEASUREMENT OF $J$

Two different techniques for measuring the spatial profile of the current density  $J$  are introduced here. In both techniques, visible light focused on a superconducting film acts as the spatial probe. In these techniques, the intensity of the probing light beam is modulated at the frequency  $f_{\text{light-chop}}$  and light energy is absorbed in the film at this same frequency. This periodic energy absorption gives rise to a periodic temperature modulation in the material underneath the light spot. *All* of the temperature dependent properties of the illuminated part of the superconductor will be modulated at  $f_{\text{light-chop}}$ . One important concern for the spatial resolution of the measurement is that the energy deposited during a light-on half-cycle will diffuse away from the light spot during the cycle. The light modulation  $f_{\text{light-chop}}$  must be rapid enough so that the thermal diffusion of heat away from the light spot within one period of the modulation cycle is not large enough to significantly reduce the spatial resolution.

We report on two techniques for measuring the spatial profile of  $J$  that rely on the temperature dependence of two different properties of the superconductor. For the kinetic-inductance bolometric technique, the property modulated is the magnetic field penetration depth  $\lambda$ . For the resistive-

transition bolometric technique, the property modulated is the film resistance. Whereas the temperature dependence of  $\lambda$  is significant at temperatures well below  $T_c$ , the temperature dependence of the film resistance is significant only for temperatures near  $T_c$ . As a consequence, the kinetic-inductance technique can be used from temperatures slightly below to temperatures well below  $T_c$ . The resistive-transition technique can be used only at temperatures within the resistive transition near  $T_c$ . The kinetic-inductance technique was used to acquire most of the data reported in this work.

### A. Measuring $J$ using the kinetic-inductance photoresponse

In this technique, the magnetic field penetration depth  $\lambda$  is the temperature dependent property of importance that is modulated at the frequency  $f_{\text{light-chop}}$ . The illuminated film spot must be part of a resonant structure or an interferometer. The case of a resonant structure is considered here. In a resonant structure, if  $\lambda$  is modulated, then the magnetic field energy stored in the resonator is also modulated. As  $\lambda$  increases, the magnetic field penetrates further into the superconductor and the total energy stored in the magnetic field increases. This increase in stored magnetic field energy causes a decrease in the resonance frequency  $f$ . The resonance frequency  $f$  of the structure (of which the spot illuminated by the light is a part) is thus modulated at the frequency  $f_{\text{light-chop}}$ . The magnitude  $\delta f$  of the modulation of  $f$  depends on the magnitude of the magnetic field at the light spot. For example, if there is no magnetic field, then there will be no change in the stored energy and thus no shift of the resonance frequency. Because the surface magnetic field is closely related to the surface current density, the measured shift in the resonant frequency contains information about the current density.

To quantify the above in terms of parameters of interest, consider the following approach: A microwave power  $P_{\text{in}}$  is input to a resonant structure and the power  $P$ , either transmitted through the structure or reflected back from the structure, is measured. The change in  $P$  caused by a light-induced change in  $T$  is

$$\delta P = \frac{\partial P}{\partial T} \delta T = \frac{\partial P}{\partial f} \frac{\partial f}{\partial T} \delta T = \frac{\partial P}{\partial f} \delta f, \quad (1)$$

where  $\delta f$  is the light-induced shift in the resonance frequency. The shift in the resonance frequency can be calculated using standard cavity perturbation theory:<sup>15</sup>

$$\frac{\delta f}{f_0} = \frac{\delta W_e - \delta W_m}{W}, \quad (2)$$

where  $f_0$  is the resonance frequency of the unperturbed structure,  $\delta W_e$  is the change in total electric field energy stored in the resonator,  $\delta W_m$  is the change in the total magnetic field energy stored in the resonator, and  $W$  is the total energy stored in the resonator. In this measurement,  $\delta W_e$  is negligible and  $\delta W_m$  can be expressed as<sup>16</sup>

$$\delta W_m = \delta \left[ \frac{1}{2\mu_0} \int B^2 + (\mu_0 \lambda J)^2 dV \right], \quad (3)$$

where the integral is over the volume occupied by the currents and fields of the resonator. The second term in the integrand is the kinetic-inductance term (i.e., the kinetic energy associated with the superconducting current). Under all conditions, this integrand is proportional to  $J^2$  and the proportionality constant is independent of position within the superconductor; this  $\lambda$  can also be associated with a magnetic field penetration depth as long as the density of Cooper pairs is independent of position. The fields external to the superconductor are insensitive to small local changes in magnetic field penetration and thus are essentially unchanged and contribute nothing to  $\delta W_m$ . The dominant change occurs in the distribution of currents and fields inside the superconductor—and specifically within the region whose temperature is being modulated.

A few simple assumptions are sufficient to simplify Eq. (3). Consider a coordinate system in which the propagation direction of the transmission line is along the  $y$  axis, the  $z$  axis is normal to the plane of the transmission line, and the  $x$  axis is directed across the width of the transmission line. The assumptions are as follows: (1) At the surface of the superconducting strip only  $B_x$  is nonzero. (2) The rate at which  $B_x$  changes with position along the transmission line is negligible compared to the rate at which it changes within the  $x$ - $z$  plane. (3) The  $B_x$  component of the magnetic field inside the superconducting film can be expressed as a product of a function of  $x$  and a function of  $z$ ; this assumption can be expected to break down for positions within  $\sim\lambda$  of the strip edge and is consistent with calculations.<sup>17–19</sup> (4) We assume that  $\mathbf{J}=(1/\mu_0)\nabla\times\mathbf{B}$  is a valid local relation (and the displacement current is negligible). With these assumptions Eq. (3) reduces to

$$\delta W_m = \frac{\mu_0}{2} (\lambda J_0)^2 g(\lambda) A \delta\lambda, \quad (4)$$

where  $J_0 \equiv J(x, y, 0)$  is the unperturbed current density at the surface ( $z=0$ ) underneath the light spot,  $g(\lambda)$  is a function of  $\lambda$  and the geometry of the transmission line,  $A$  is the area illuminated, and  $\delta\lambda$  is the light-induced shift in  $\lambda$ . As a special case, consider a film thick compared to  $\lambda$  where the magnetic field and the current decay exponentially into the film. In this case, the two components of the integrand in Eq. (3) contribute equally and  $g(\lambda)=1$ . In general,  $g(\lambda)$  is not a constant and the kinetic-inductance term makes the larger contribution to  $\delta W_m$ . If the assumptions used to get Eq. (4) from Eq. (3) are not valid or if a more precise interpretation of  $\delta P$  is needed for positions within  $\lambda$  of the edge of the strip, then the integral in Eq. (3) must be re-evaluated using a model for the field and current distributions.

Combining Eqs. (1), (2), and (4) the kinetic-inductance photoresponse is

$$\delta P = - \frac{\partial P}{\partial f} f_0 \frac{\mu_0}{2} \frac{(\lambda J_0)^2}{W} g(\lambda) A \delta\lambda. \quad (5)$$

If the modulation  $\delta P$  is measured for  $f$  on the shoulder of the resonance where  $\partial P/\partial f$  is largest, and the light spot is translated around the film, then  $\delta P$  will map out  $J_0^2$ , because none of the other parameters in Eq. (5) change with position. In making this conclusion we assume that neither  $T_c$  nor the

light-induced temperature rise  $\delta T_{\text{local}}$  vary significantly with position. The assumptions made to derive Eq. (5) are valid for most of the measurements presented in this work.




An additional assumption in the analysis above is that the light-induced temperature rise in the film is uniform through the thickness of the film. When the period of the light modulation is on the order of the time that it takes a heat pulse to traverse the film thickness, this assumption is no longer valid. Assuming diffusive transport, and using thermal conductivity<sup>20</sup> and heat capacity<sup>21</sup> measurements reported for YBCO, the diffusion length for one-dimensional diffusion at 90 K decreases to  $\sim 0.5 \mu\text{m}$  when the light modulation frequency is increased to 40 MHz. The light-modulation frequencies used in the measurements reported here ( $f_{\text{light-chop}} \sim 0.5$  MHz) were much smaller, so it is reasonable to assume a uniform temperature rise through the thickness of the film. If measurements are performed at high frequencies it is possible to probe the distribution of current on opposing surfaces of the film or through the thickness of the film. This can be done by repeating measurements for light incident on opposite sides of the superconducting film (given a transparent substrate) or by repeating the measurements as a function of the light modulation frequency.

The quadratic dependence of the photoresponse  $\delta P$  on the current density  $J$  in Eq. (5) is an important advantage. It allows easy detection of changes in the spatial profile of  $J$  that occur on distance scales much smaller than the spatial resolution of the photoresponse measurement. Consider a light beam focused on a current peak at the edge of a superconducting strip and assume that Eq. (5) is valid to a reasonable approximation at this edge. Approximate this current peak as a rectangle of height  $J$  and width  $W$  where  $W < 1 \mu\text{m}$  is much narrower than the  $6.6 \mu\text{m}$  resolution of a typical photoresponse measurement in this work. The contribution to  $\int J(x)^2 dx$  of the rectangular current peak to the photoresponse is  $J^2 W$ . If the current peak is reduced in height by a factor of 2 and broadened by a factor of 2, it contains the same total current, but the photoresponse changes to  $(J/2)^2 (2W) = J^2 W/2$ . Because  $J$  is sharply peaked at the edges of superconducting strips, the photoresponse measured at these edges is dominated by the edge current.

## B. Measuring $J$ using the resistive-transition photoresponse

In this technique, the resistive loss of the superconducting film is the temperature dependent property of importance that is modulated at the frequency  $f_{\text{light-chop}}$ . The temperature of the film is set within the resistive transition where the transmitted microwave power  $P$  changes rapidly with temperature. Consider the light-induced change  $\delta P$  in the transmitted power. If the magnitude of the temperature modulation  $\delta T$  is small, the current distribution will not be perturbed significantly. Consider the change in the dissipated power. Only the region inside the superconductor underneath the light spot contributes to the change in dissipation. If this

TABLE I. Fifty  $\Omega$  transmission-line resonator samples.

Sample	Superconductor /substrate	Planar technology	Device geometry	Strip width ( $\mu\text{m}$ )	Fundamental resonance (GHz)
1	$\text{Ti}_2\text{Ba}_2\text{CaCu}_2\text{O}_8$	Coplanar	 Side-coupled rectangular loop (notch filter)	30	1.5
2	$\text{YBa}_2\text{Cu}_3\text{O}_{7-\delta}$ /LaAlO <sub>3</sub>	Coplanar	 Side-coupled rectangular loop (notch filter)	30	1.5
3	$\text{YBa}_2\text{Cu}_3\text{O}_{7-\delta}$ /LaAlO <sub>3</sub>	Microstrip	 Side-coupled square loop (notch filter)	150	4
4	$\text{YBa}_2\text{Cu}_3\text{O}_{7-\delta}$ /MgO	Microstrip	— — — End-coupled resonator	500	6.25

region has a current  $I$  running through it and the change in the local resistance is  $\delta R_D$ , then (neglecting reflectance changes)

$$\delta P = -I^2 \delta R_D. \quad (6)$$

If the resistive properties of the superconducting film are spatially uniform (or vary much more slowly with position than does the current density), then the measurement of the light-induced change in the transmitted microwave power will map out the square of the current density as the light spot is translated over the surface of the superconductor. Just as was the case for the kinetic-inductance technique, measurements using this technique allow us to determine the spatial profile of the current distribution on a superconducting surface. This resistive-transition photoresponse techniques shares the same advantage discussed above for the kinetic-inductance photoresponse technique, because it also measures a quantity proportional to the square of the current density. A low spatial resolution dc current version of this technique using a laser excited phonon beam to probe the superconducting current has been done by Kent and Chapman.<sup>22</sup>

### III. FILMS AND DEVICES

Measurements were performed on four transmission line devices: two coplanar and two microstrip. Most of the measurements were performed on the coplanar devices—samples 1 and 2 in Table I. Except for film material (TBCCO for sample 1 and YBCO for sample 2) and film thickness, the coplanar devices were identical to each other. The devices (notch filters) were “rectangular” loops into which energy was coupled from an adjacent transmission line (see Fig. 1). Both films were grown on LaAlO<sub>3</sub> substrates of thickness 0.508 mm. The 50  $\Omega$  coplanar transmission lines had 30  $\mu\text{m}$  wide center strips separated by 58  $\mu\text{m}$  wide gaps from the ground planes. The 1.56 cm  $\times$  1.30 cm rectangular loop had a circumference of 5.72 cm and a fundamental resonance frequency of 1.5 GHz. The coupling gap between the input line and the adjacent loop was 200  $\mu\text{m}$ . The ground planes were interconnected by gold wire bonded to gold pads.

The TBCCO film of sample 1 was grown using an *ex situ* technique on a 2 in. diam LaAlO<sub>3</sub> wafer. The surface

roughness of this film was on the order of 1000  $\text{\AA}$ . It had platelike grains of irregular shape whose lateral sizes were  $\sim 5 \mu\text{m}$ .<sup>23</sup> The film was  $0.65 \pm 0.05 \mu\text{m}$  thick with a typical microwave surface resistance of  $< 200 \mu\Omega$  at 80 K and 10 GHz, and a lower critical magnetic field  $H_{c1} \sim 10$  Oe (which corresponds to  $J \sim 4 \times 10^5 \text{ A/cm}^2$ ). Typically, current densities of  $\geq 2 \times 10^6 \text{ A/cm}^2$  have been measured at 70 K on similar unpatterned films.

Sample 2 was an identical coplanar transmission-line resonator fabricated using YBCO film grown on a 2 in. diam LaAlO<sub>3</sub> wafer.<sup>23</sup> The grain size of the YBCO film was small compared to that of the TBCCO film with a surface roughness of  $\sim 100 \text{\AA}$ . The film was  $0.45 \mu\text{m}$  thick with a typical microwave surface resistance of  $< 300 \mu\Omega$  at 80 K and 10 GHz, and a lower critical magnetic field of  $H_{c1} \sim 10$  Oe. Typically, current densities of  $\geq 5 \times 10^6 \text{ A/cm}^2$  have been measured at 70 K on similar unpatterned films.

Two 50  $\Omega$  YBCO microstrip transmission line resonators (samples 3 and 4) were also fabricated and used in this work. For the measurements performed on these devices, the light intensity was modulated at  $f_{\text{light-chop}} = 100 \text{ kHz}$  using a photoelastic modulator (as opposed to the acousto-optic modulator discussed below that was used for the coplanar devices).

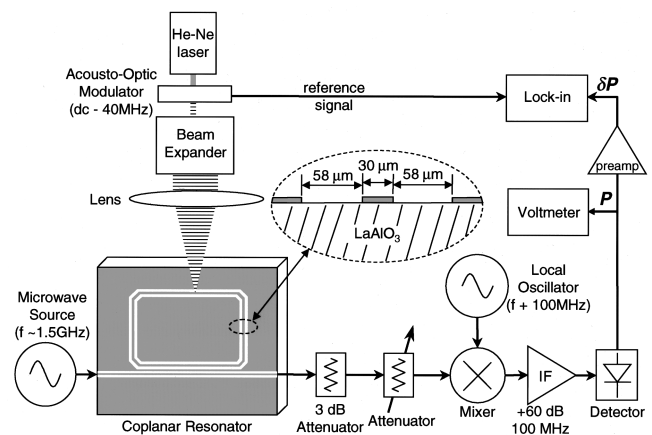


FIG. 1. A schematic of the optical and electronic setup.

The first microstrip device, sample 3, was a notch filter. It was a square loop with impedance matched mitered corners into which energy was coupled from an adjacent transmission line. This device was fabricated on a 0.508 mm thick  $\text{LaAlO}_3$  substrate. The 0.2  $\mu\text{m}$  thick YBCO film was grown using a pulsed laser deposition technique.<sup>24</sup> The grain size of this film was  $\sim 1 \mu\text{m}$ . All lines were 150  $\mu\text{m}$  wide. The ground plane was a 3  $\mu\text{m}$  thick film of metallic Ag that was deposited onto the opposite side of the substrate by evaporation. The fundamental resonance frequency of the square loop was 4 GHz. The kinetic-inductance photoresponse measurements shown here were conducted using a microwave frequency set to the second harmonic (8 GHz).

The second microstrip device, sample 4, was a simple end-coupled microstrip resonator fabricated on a 0.508 mm thick MgO substrate using a metalorganic chemical vapor deposition technique.<sup>25</sup> The resonator was 8.94 mm long, coupled by 0.5 mm gaps at the ends. The width of the microstrip line was 500  $\mu\text{m}$ . This resonator was designed to have its first harmonic at 6.25 GHz.

#### IV. EXPERIMENTAL SETUP

Figure 1 shows a schematic of the optical and electronic setup used in this experiment to study samples 1 and 2. The setup used to study samples 3 and 4 differed only in that a 100 kHz photoelastic modulator was used instead of the acousto-optic modulator. The rectangular slab represents a coplanar resonator sample. Microwave source was connected to one side of the device and the microwave power  $P$  transmitted through to the other side was measured. Light was focused onto the sample and the change in the transmitted microwave power  $\delta P$  (the photoresponse) was measured.

About 1 mW of the He-Ne laser's 2 mW output power reached the sample after passing through an acousto-optic modulator, a beam expander, and a focusing lens. During each cycle of modulation, the light power reaching the sample oscillated between zero and 1 mW. For most measurements of the coplanar devices,  $f_{\text{light-chop}}$  was between 0.3 and 0.5 MHz.

For kinetic-inductance photoresponse measurements, the light was focused onto part of the resonator. For measurements done at a fixed microwave frequency,  $\delta P$  was maximized by setting the microwave frequency at an inflection point of the resonance  $P(f)$ . The magnitude of the light-induced modulation  $\delta f$  of the resonance frequency was always small compared to the width of the resonance. For  $f_{\text{light-chop}} = 0.52 \text{ MHz}$ , the resonance shift for the YBCO sample was  $\delta f = \delta P / (\partial P / \partial f) = 17 \text{ Hz}$  at 55 K, and  $\delta f = 1 \text{ kHz}$  at 80 K (80 K was  $\sim 2 \text{ K}$  below the low  $T$  side of the resistive transition).

For resistive-transition measurements, the light was focused not on the loop, but on the input transmission line, and the microwave frequency was chosen to be far from any resonance.

The microwave electronics detection system was as follows. A variable attenuator was used to limit the microwave power delivered to the mixer. The signal was mixed down to an intermediate frequency of 100 MHz, amplified, and de-

tected. Both the dc and light-modulation components of the signal were recorded. The component of the signal synchronous with the reference signal from the acousto-optic modulator—the photoresponse—was extracted using a high-frequency lock-in amplifier.

The ultimate spatial resolution that can be achieved using this technique is equal to the minimum spot size to which the probing light can be focused. This resolution can be realized only if the light intensity is modulated fast enough so the “hot spot” is not significantly broadened by thermal diffusion during one cycle of the light modulation. Optimal focusing occurs for well-collimated light beams when the radial intensity distribution is Gaussian.<sup>26</sup> The minimum beam radius  $r_e$  that can be achieved for light of wavelength  $\lambda_{\text{opt}}$  being focused down in a cone of half-angle  $\theta$  is determined by  $\tan(\theta) = (\lambda_{\text{opt}}/n)/(\pi r_e)$ , where  $n$  is the index of refraction of the medium in which the minimum focus is occurring, and  $\theta$  is measured from cone center out to where the electric field of the incident light beam drops by  $1/e$ . For the experiments reported here  $\lambda_{\text{opt}} = 0.6328 \mu\text{m}$ ,  $n = 1$ , and  $\tan(\theta) = 0.055$ , so  $r_e = 3.7 \mu\text{m}$ . Generally, the photoresponse depended linearly on the light energy absorbed and thus quadratically on the electric field, so 3.7  $\mu\text{m}$  is the  $1/e^2$  point for the power; that the signal depends on light power rather than field improves our spatial resolution by a factor of  $2^{-1/2}$ . The optimum spatial resolution for our experimental geometry corresponds to a full width at half maximum (FWHM) = 4.4  $\mu\text{m}$  for the photoresponse measurements.

A typical spatial resolution determined from the photoresponse measurements shown below is FWHM = 6.6  $\mu\text{m}$ . This FWHM is 50% larger than that expected for a beam limited by Gaussian optics. We attribute the nonoptimal spot size to vibrations of the apparatus.

#### V. BASIC MEASUREMENTS—VALIDITY CHECK

One goal of this work is to study the effect that increasing microwave power has on the distribution of current on a superconducting strip (Sec. VI). It is therefore important to explore how other experimental parameters affect the photoresponse measurements so that we can correctly identify the behaviors that are caused by the increase of microwave power. It is also important to determine to what degree the act of making a measurement alters the system being measured. Finally, it is important to understand the nature of the changes in the photoresponse that we expect to observe as parameters such as temperature are changed. The remainder of this section deals with these issues.

After discussing the basic kinetic-inductance photoresponse measurements and noting the existence of enhanced photoresponse signals from intergranular regions, we present photoresponse data measured for different temperatures and light powers. We present observations near  $T_c$  that show that high light power alters the shape of both kinetic-inductance and resistive-transition  $\delta P(x)$  for both YBCO and TBCCO. Finally, the local light-induced temperature rise is calculated from both resistive-transition and kinetic-inductance photoresponse measurements. These calculations provide an esti-

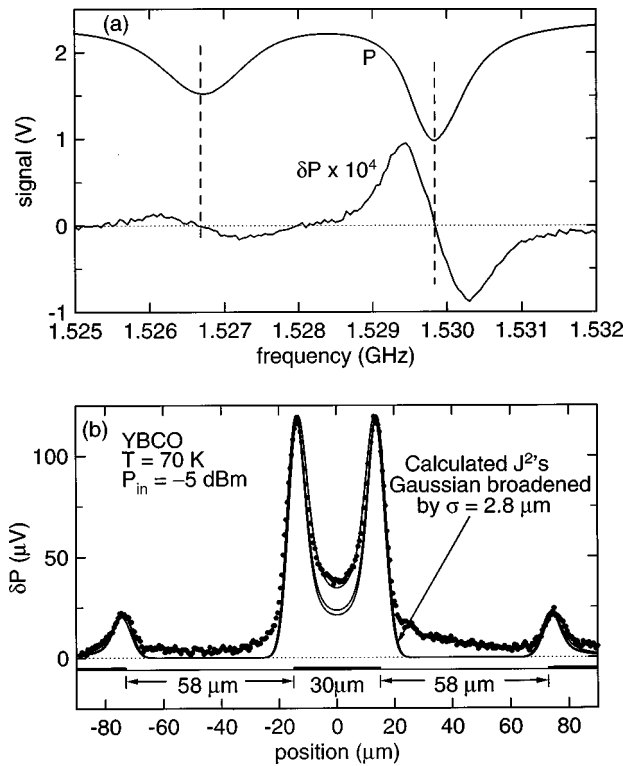


FIG. 2. Coplanar YBCO notch filter (sample 2). These measurements were performed at 70 K using a modest incident microwave power of  $P_{in} = -5$  dBm. (a) Transmitted microwave power  $P$  and light-induced modulation of the transmitted power  $\delta P$  plotted as a function of the microwave frequency. Two resonances are seen. Note that  $\delta P \propto \partial P / \partial f$ . (b) The dots are a measurement of  $\delta P(x)$  across the transmission line from one ground plane to the opposite ground plane. The three solid lines are theoretical  $\delta P$  determined from numerical calculations of the current distribution in a homogeneous dielectric media version of this coplanar structure (courtesy of Howard Snortland). Plotted from top to bottom are the surface currents for  $\lambda = d, d/2$ , and  $d/3$ , where  $d = 0.45 \mu m$  is the thickness of the superconducting film.

mate of the degree to which the act of measurement is perturbing the system being measured.

### A. YBCO photoresponse

Several of the first measurements on the coplanar YBCO resonator (sample 2) are shown in Fig. 2 for 70 K. Two fundamental resonances are seen in Fig. 2(a). The standing wave patterns corresponding to these two resonances are orthogonal—where one resonance has current peaks along the strip, the other has current zeros. The degeneracy of the resonances has been removed by the effect the different mode field patterns have on the group velocity along the coupling leg of the loop. The standing wave having the higher current density at the power input side of the loop corresponds to the higher frequency resonance.

The photoresponse  $\delta P(f)$  in Fig. 2(a) looks like a derivative of the resonances in the  $P(f)$  curve—as expected from Eq. (1). The photoresponse is much larger for the higher frequency resonance. This means that the position of the light spot along the strip is close to a peak in the standing wave for the higher-frequency resonance. All data were taken at the first harmonic of the loop; at this resonant fre-

quency, there are two cycles of  $J^2$  or  $720^\circ$  around the loop. All other measurements shown here for the YBCO sample 2 were taken with the light spot moved closer to the peak of the standing wave. We estimate that no data were taken further away than  $3/4$  mm or  $10^\circ$  away from the peak, and most were within  $1/4$  mm or  $3.3^\circ$ . For the TBCCO data discussed in the next section, all measurements were acquired so close to the peak as to be indistinguishable from the peak.

The photoresponse  $\delta P(x)$  measured while translating the light spot across the coplanar transmission line from ground plane to ground plane is shown in Fig. 2(b). To help associate the photoresponse features with the physical features of the transmission line, a schematic showing the location of the superconducting film is included below the photoresponse. The photoresponse has peaks near every superconducting film edge. From Eq. (5), the photoresponse is expected to be proportional to the square of the current density, suitably broadened by the finite spatial resolution of the measurement (resolution  $FWHM \approx 6.6 \mu m$ ). The magnetic fields in the transmission line around the  $30 \mu m$  wide center strip are largest near the strip edges. The currents that are established within the superconducting film to screen these fields should be largest at edges of the strip; this expectation is satisfied by the photoresponse.

The three solid lines shown in Fig. 2(b) are the result of calculations<sup>17–19</sup> of the current density across the coplanar transmission line. In these calculations the dielectric medium was assumed to be homogeneous; for the devices studied here, the dielectric medium is inhomogeneous. Calculations were performed for penetration depths of  $\lambda = d/3, d/2$ , and  $d$ , where  $d = 0.45 \mu m$  was the film thickness. Low microwave power conditions were assumed. The calculated  $J(x)$  were squared, convolved with a Gaussian characteristic of the spatial resolution of the measurement, and scaled to have the same amplitude as the measurement. Note the excellent agreement between the measured  $\delta P(x)$  and the  $\delta P(x)$  inferred from the calculation in which  $\lambda = d$  was assumed; a penetration depth of  $\lambda = 0.45 \mu m$  at 70 K is not unreasonable for an epitaxial YBCO film whose  $T_c \sim 84.5$  K. The calculations using the two smaller  $\lambda$ 's yielded almost identical current distributions that are more peaked at the edges. In all three calculations, the relative magnitudes of the current peaks on the strip relative to those on the ground planes were in excellent agreement with the measured  $\delta P(x)$ .

When light is focused onto one of the gaps in the superconducting film, a small photoresponse is seen. This photoresponse exists because some of the light that enters the substrate reflects off its back surface and gets absorbed at the underside of the superconducting film [see Fig. 3(a)]. The light beam (having reached its focal point at the plane of the superconductor) diverges as it travels into the transparent  $LaAlO_3$  substrate. The beam reflected back to the underside of the film beam has a  $FWHM \sim 26 \mu m$ . We observed that when the light beam was tilted away from normal incidence to increase the light undershoot at one side of the  $30 \mu m$  wide strip, the light undershoot at the other side of the strip was correspondingly reduced. This behavior is illustrated in Fig. 3(b) using the  $150 \mu m$  wide YBCO microstrip sample (sample 3). This effect was smaller for the coplanar trans-

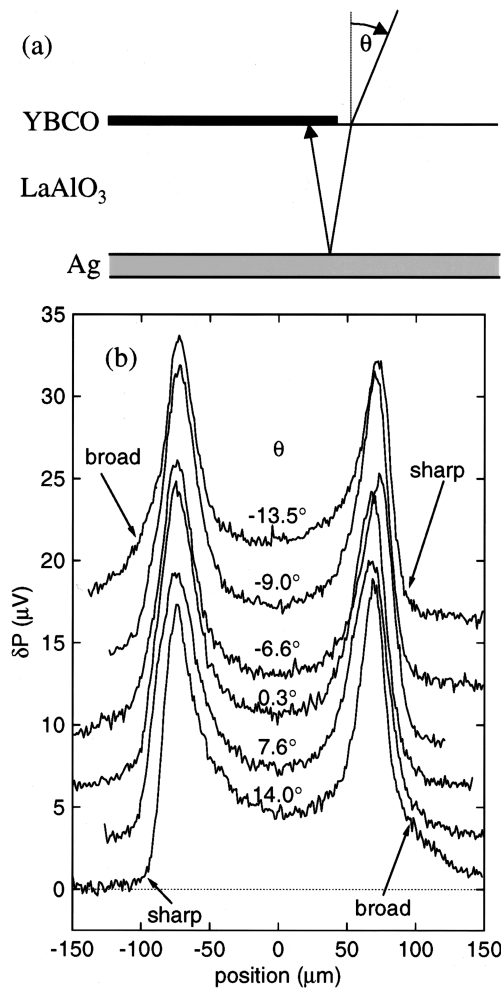


FIG. 3. Effect of the diverging light beam back reflecting to underside of the superconducting strip. (a) Schematic of the edge of a superconducting film deposited on a dielectric slab with light ray incident at angle  $\theta$ . (b) Photo-response  $\delta P$  measured across a  $150\text{ }\mu\text{m}$  wide YBCO microstrip line (sample 3) for six different angles of incidence of the probing light beam. Note the shoulders on  $\delta P$  that are seen under conditions where the under-shoot of light is expected.

mission lines compared to the microstrip transmission lines; our microstrip transmission lines have reflective metallic films deposited on the backside of the substrate so a larger fraction of the light entering the substrate was reflected back to the plane of the superconducting film.

When kinetic-inductance photoresponse measurements were performed in which the light spot was translated across the power input segment of coplanar line, no photoresponse was seen—except for a small resonant current on the edge of the ground plane closest to the rectangular loop.

## B. TBCCO photoresponse

The resistive transition of the coplanar TBCCO device (sample 1) is shown in the inset in Fig. 4. Arrows indicate the temperatures at which first harmonic resonances shown in Fig. 4 were measured. Just as for YBCO sample 2, there are two nearly degenerate resonances that correspond to the first harmonic of the loop. As  $T \rightarrow T_c$ , the resonances degraded dramatically, but because the temperature depen-

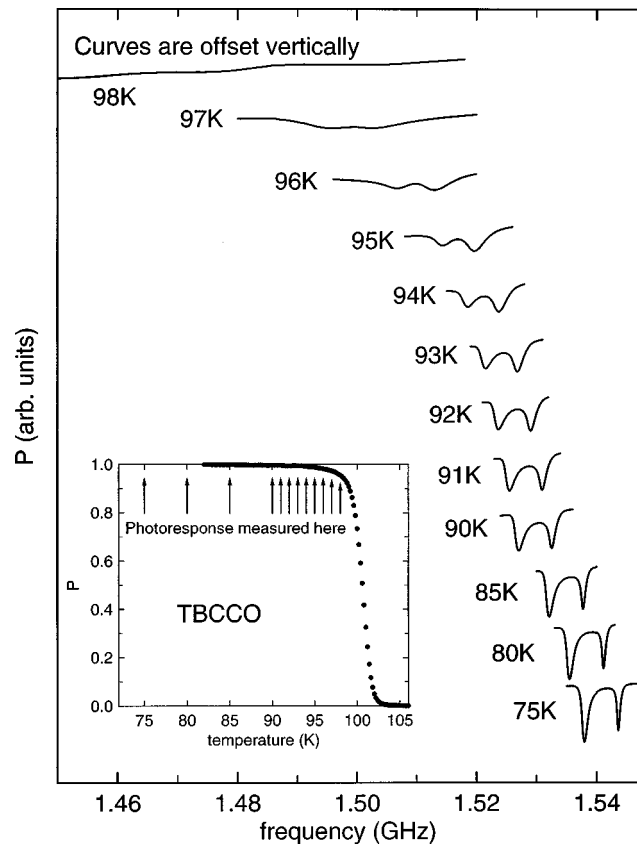


FIG. 4. TBCCO notch filter (sample 1). First harmonic resonances vs temperature. Inset shows the transmitted microwave power  $P$  measured as the temperature passed through the resistive transition. Arrows show the temperatures where the resonances were measured. Kinetic-inductance photoresponse was measurable at all of these temperatures. The incident microwave power was  $-8\text{ dBm}$ .

dence of the magnetic field penetration depth  $\lambda$  increases rapidly, a measurable kinetic-inductance photoresponse was observable at temperatures up to 98 K.

Figure 5(a) shows the transmitted microwave power  $P$  and the photoresponse  $\delta P$  that were measured as the microwave frequency was scanned through the first harmonic of the resonant loop at 90 K. Note that a nonzero  $\delta P$  was observed only for the lower of the two resonances. In this measurement the light spot was positioned along the strip at a peak in the current standing wave of the lower frequency resonance and thus at a zero in the current standing wave of the upper frequency resonance. The standing wave patterns for these two resonances are orthogonal. Measurements of portions of these standing waves are shown in Fig. 6(a) with a schematic of the resonator. The solid-line  $\delta P$  data shown slightly above two legs of the loop were measured while scanning the light spot along the strip with the microwave frequency set on the shoulder of the lower resonance. Measurements performed with the microwave frequency set on the shoulder of the upper resonance are plotted as dotted lines. The orthogonality of these standing wave modes is apparent.

The  $\delta P$  measurements in Fig. 6(a) clearly show a standing wave pattern, but there is nothing in this data that proves that the signal measured is proportional to the square of the

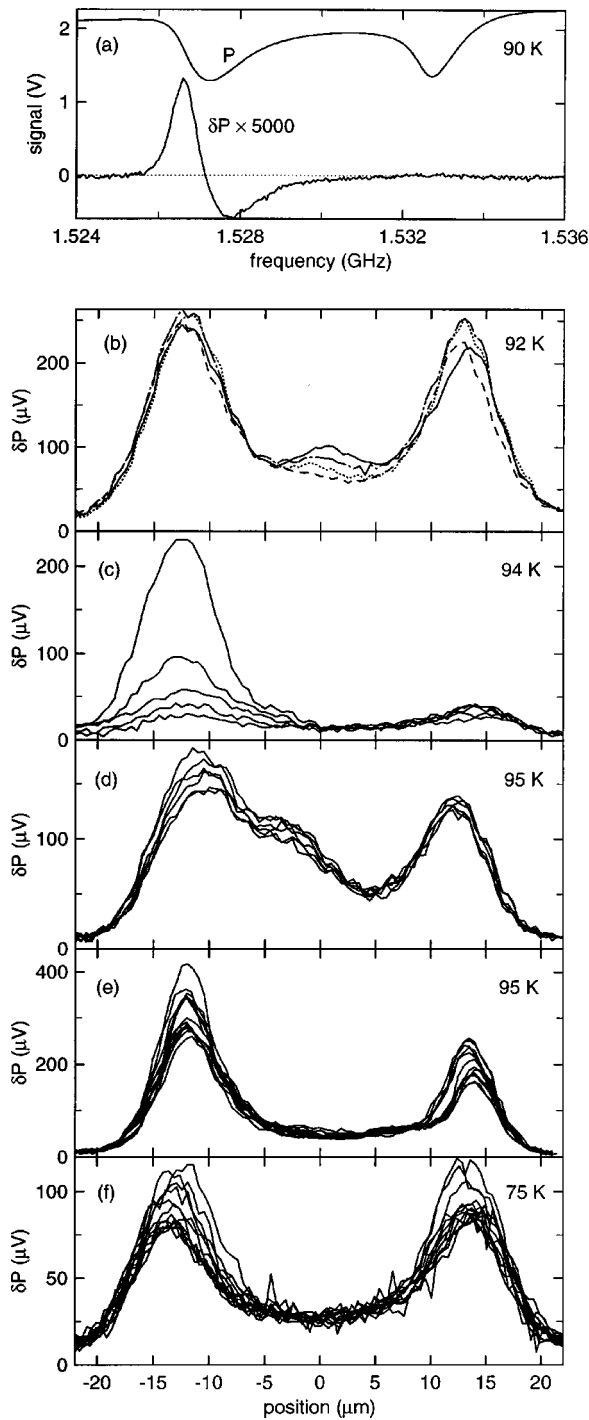


FIG. 5. Measured photoresponse  $\delta P$  of the coplanar TBCCO sample 1. The light power incident on the sample was 1 mW for all data in this figure except for (c) where 0.4 mW was used. (a) Transmitted microwave power  $P$  and the photoresponse  $\delta P$  measured at 90 K plotted as a function of microwave frequency  $f$ . Two slightly nondegenerate fundamental resonance modes exist. The predicted  $\delta P \propto \partial P / \partial f$  character is clearly evident. A photoresponse is seen only for the lower frequency mode, because the light spot was moved along the coplanar transmission line until the photoresponse from the low frequency mode reached maximum and consequently the photoresponse from the high-frequency mode became zero. The multiple  $\delta P(x)$  traces displayed in parts (b) through (f) were measured with scan paths spaced apart by several microns along the strip: (b) 92 K, (c) 94 K, (d) 95 K, (e) 95 K [at different position than (d)], and (f) 75 K.

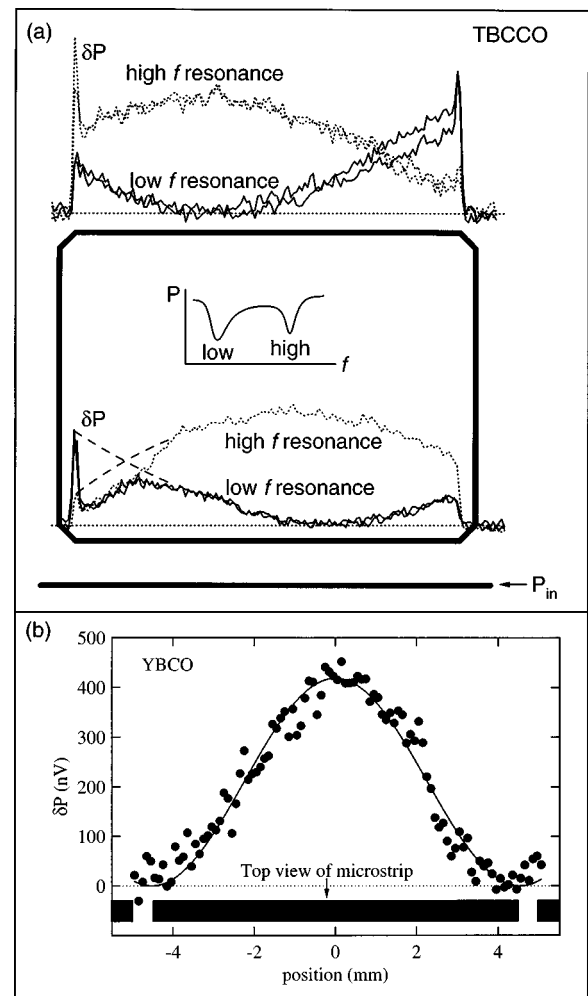


FIG. 6. Measured current standing waves. (a) Schematic of the TBCCO coplanar resonator (sample 1) with the measured photoresponse  $\delta P$  plotted above the sides of the loop along which they were measured. The light beam was defocused to a diameter of 120  $\mu m$  and translated along the strip. The  $\delta P$  (plotted as a solid lines and dotted lines) were measured with the microwave frequency on the shoulder of the low and high frequency resonances, respectively. The two fundamental resonances, measured at 85 K, are plotted inside the resonator loop. Deviations from an ideal measurement occurred when the laser beam scan path was not centered on and absolutely parallel to the 15.6 mm long leg. At the ends of the  $\delta P(x)$  measurements where sharp peaks were observed, the laser beam path was off the center of the 30  $\mu m$  wide strip toward the inside of the loop; the sharp peaks were measured as the laser beam passed over the 45° corner parts of the loop. (b)  $\delta P(x)$  measured along an end-coupled YBCO microstrip resonator (sample 4). Beneath the  $\delta P(x)$  measurement is a top view of the resonator. Only one first-harmonic resonator exists for this device. This  $\delta P(x)$  measurement proves that  $\delta P$  is a measure of the current (as opposed to voltage) standing wave.

current as opposed to the square of the voltage. The possible existence of another photoresponse mechanism, one associated with the voltage standing wave, must be considered. To experimentally address whether the modal structure seen in the photoresponse is associated with current or voltage standing waves, we performed measurements on a microstrip device patterned as an end-coupled resonator (sample 4)—a geometry for which no ambiguity exists. See Fig. 6(b) for both the photoresponse data and a top view of the end-coupled microstrip transmission line geometry. For this system, only one first harmonic resonance exists and the current



for its standing wave must be zero at the gaps and at maximum in the middle of the strip between the two gaps. The voltage in the standing wave has maxima at the gaps and a minimum in the middle. The data clearly indicate that the photoresponse is proportional to the square of the current, not the voltage. The solid line through the data is a fit to  $\cos^2(kx + \phi)$ —consistent with  $\delta P$  being proportional to  $J^2$ .

The measurements of  $\delta P(x)$  across the TBCCO coplanar transmission line [see Figs. 5(b)–5(f)] show large variations in shape along the transmission line; this is in distinct contrast to the YBCO samples which showed negligible variations. Where multiple curves are plotted together in Figs. 5(b)–5(f), the light spot paths used to acquire the curves were translated several microns along the strip from each other. For all of the scans shown in Fig. 5 the light spot was positioned along the strip at a point corresponding to the peak in the standing wave for the lower frequency resonance and a zero in the standing wave for the upper frequency resonance. All of the  $\delta P(x)$  data for TBCCO discussed below in this article were measured with the light spot positioned so that there was no measurable photoresponse corresponding to the upper resonance.

A peak near the middle of the strip is clearly visible in the 92 K measurements of the photoresponse  $\delta P(x)$  that are shown in Fig. 5(b). These data are strikingly different from the measurements made on YBCO sample 2; no peaks in  $\delta P$  between the edge-peaks were ever seen for YBCO sample 2. The small central  $\delta P$  peak occurs at slightly different positions in each measurement and the width of the central peak is limited by the spatial resolution of the measurement (FWHM  $\sim 6.6 \mu\text{m}$ ). Compared to YBCO sample 2, the edge-peaks for this set of data fell more rapidly as the light spot was scanned from the edge toward the center of the strip; this behavior became even more pronounced at higher temperatures [see Fig. 5(e)].

For distance scales on the order of several microns along the strip, the variation in the height of the edge-peaks in the TBCCO sample 1 was much larger than for YBCO. Figure 5(c) shows measurements of  $\delta P(x)$  made at 94 K. This region of the strip had the largest spatial variation in  $\delta P$  that we observed. Keeping temperature constant, measurements at this location for different light-modulation frequencies and light powers did not effect the variation in the height of the edge-peaks.

Substantial photoresponse peaks not located at the strip edges became more prevalent as the temperature approached  $T_c$ . The measurements of  $\delta P(x)$  at 95 K shown in Figs. 5(d) and 5(e) for two regions along the transmission line illustrate typical behavior. A substantial peak in  $\delta P$  is seen between the two edge-peaks in Fig. 5(d). Figure 5(e) shows similar measurements of  $\delta P(x)$  made at 95 K for a nearby part of the strip; the sharper edge-peaks and the flatter  $\delta P$  between the peaks were typical for regions containing no  $\delta P$  peaks between the edge-peaks.

At lower temperatures, variations at the strip edges were still observed, but no additional peaks were ever seen between the two edge-peaks. The thirteen  $\delta P(x)$  curves measured at 75 K that are shown in Fig. 5(f) illustrate the typical behavior. The smoother shape of the  $\delta P(x)$  curve between

the two peaks is more reminiscent of the measurements for YBCO.

The distance scale over which the spatial variations in  $\delta P$  occurred in the TBCCO sample 1 was on the order of 5  $\mu\text{m}$ . This value coincides with the grain size in TBCCO films as observed from scanning electron micrographs. The grain size of the YBCO film was, by contrast, much smaller. We associate the spatial variations of  $\delta P$  in TBCCO with the grain morphology of the film. The magnitudes of the  $\delta P$  fluctuations were observed to increase as  $T \rightarrow T_c$ . Peaks in  $\delta P$  between the edge-peaks were observed only for  $T \gtrsim 90$  K. The increased sharpness of the edge  $\delta P$  and the flatness of the central  $\delta P$  region were observed to lessen as  $T$  was lowered.

In the rest of this article, when it is desired to study the *intrinsic* current distribution as opposed to the *extrinsic* (grain boundary associated) current distribution, averages will be made of many  $\delta P(x)$  measured at slightly different positions along the strip; this has been done to average out the contributions of the intergrain regions.

### C. Effects of temperature and light power

Before proceeding further, it is instructive to carefully consider what we should expect to observe and what we should not expect to observe in photoresponse measurements. These comments provide a framework from which to consider the changes that are observed as temperature and light power are varied. They are also pertinent to the study of the effects of high microwave power.

Under conditions where no critical currents or fields are exceeded and where the currents are well described as surface currents ( $J < J_c$ ,  $H < H_{c1}$  and film thickness  $\lambda \ll d$ ), the distribution of the magnetic fields and currents across the strip are determined by the geometry of the transmission line (i.e., the width of the strip, the thickness of the substrate, the dielectric constant of the substrate, etc.). If changes in  $J$  (and thus  $H$ ) or  $\lambda$  are made such that the above conditions are still satisfied, then the shapes of the transverse field and current distributions across the width of the superconducting strip will remain unchanged—except within  $\sim \lambda$  of the edge. The distribution of current through the thickness of the strip is determined by the thickness of the film and the magnetic field penetration depth  $\lambda$ . Except within  $\sim \lambda$  of the edges of the strip, the shape of the current distribution through the depth of the strip is the same everywhere across the width of the strip. If the temperature is changed, then  $\lambda$  changes, and the shape of the current distribution through the thickness of the film changes everywhere uniformly—except within  $\sim \lambda$  of the edges. Experimentally, this means that the shape of the photoresponse measured across the strip will not change—except within  $\sim \lambda$  of the edges. Consider the effect that a change in  $\lambda$  has on the magnitude of the photoresponse [ $\delta P \propto (\lambda J_0)^2 g(\lambda) \delta \lambda$ , see Eq. (5)]. In the limit of current flowing on a thick superconductor,  $g(\lambda) = 1$ , and the current density (integrated through the thickness) flowing along superconductor is simply  $\lambda J_0$  per unit width. The change in the magnitude of  $\delta P$  with temperature that occurs under these circumstances occurs not through the dependence on  $\lambda$ , but

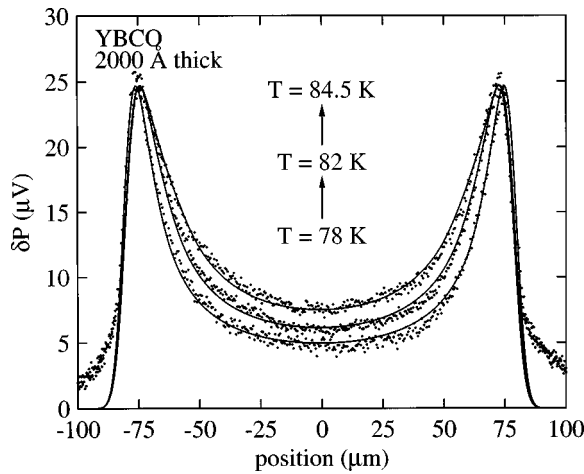


FIG. 7. Flattening, as  $T \rightarrow T_c$ , of the photoresponse  $\delta P(x)$  for a thin (2000 Å thick) YBCO microstrip transmission line (sample 3).  $\delta P$  measured across 150  $\mu\text{m}$  wide microstrip transmission line for the temperatures: 78, 82, and 84.5 K (the middle of the resistive transition was  $\sim 86.5$  K). The intensity of the light source was modulated at 100 kHz. The solid lines are fits included to help guide the eye. To emphasize the change in shape, these curves were stretched to have the same peak height as the 84.5 K measurement.

rather on the increase in  $\delta\lambda$  that occurs for the same temperature rise  $\delta T$ .

When a critical current or field is exceeded, or when the current is not well described as a surface current, then the transverse field and current distributions will change.

If  $\lambda \sim d$ , then the magnetic field penetrates through the superconducting strip sufficiently to change the field geometry of the transmission line and thus the current distribution. Theoretical calculations<sup>17</sup> [solid lines in Fig. 2(b)] and experimental measurements (Fig. 7) show that as  $\lambda$  increases, the shape of  $\delta P(x)$  becomes flatter and less peaked at the strip edges. In the theoretical calculations<sup>17</sup> of  $\delta P(x)$  shown in Fig. 2(b) only a small flattening of the current distribution was calculated to occur as  $\lambda$  increased from  $d/3$  to  $d/2$ . However, when  $\lambda$  was increased to  $\lambda = d$  a substantial flattening was calculated. This behavior is seen experimentally in Fig. 7 which shows  $\delta P(x)$  data measured for three temperatures near  $T_c$ . We attribute the measured change in the shape of  $\delta P(x)$  with temperature to the increasing magnetic field penetration that occurs as  $T \rightarrow T_c$ ; the observed increasing rate of this change in shape is consistent with the behavior expected for field penetration as  $T \rightarrow T_c$ .

The effects of the conditions  $J \sim J_c$  and  $H \sim H_{c1}$  will be realized first at the edges of the strip where the currents and fields are largest. Recall from the discussion above, that because the photoresponse is proportional to  $J^2$  (and not  $J$ ), these photoresponse measurements can reveal changes in the current distribution at the edges of the strip that occur over distance scales much shorter than the spatial resolution of the measurements.

### 1. YBCO kinetic-inductance photoresponse versus temperature and light power

Figure 8(a) shows the affect on  $\delta P(x)$  of changing the temperature of the coplanar YBCO sample 2. The behavior is substantially different from that observed in Fig. 7 (sample

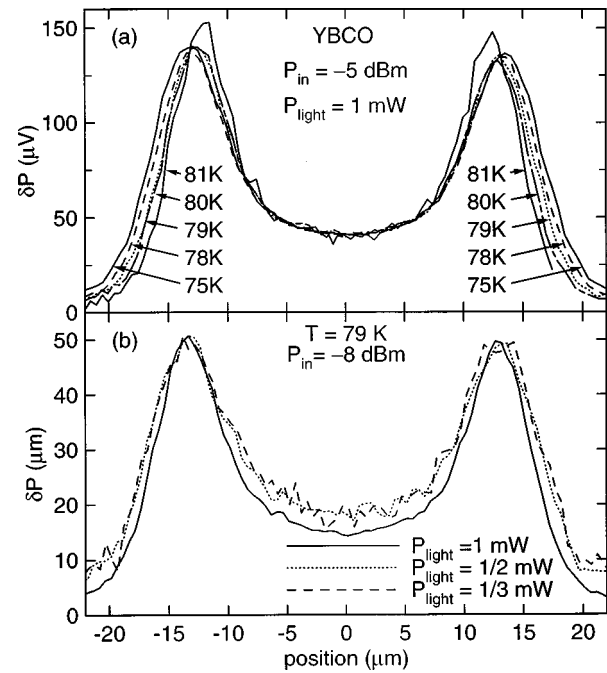


FIG. 8. Narrowing of photoresponse  $\delta P(x)$  for coplanar YBCO sample 2 with increasing light power (a)  $\delta P(x)$  measured for the temperatures 75, 78, 79, 80, and 81 K and scaled to have the same center amplitude. Peak incident light power 1 mW. Incident microwave power  $P_{\text{in}} = -5$  dBm. As  $T \rightarrow T_c$  the width of the measured  $\delta P(x)$  curves decreases. (b)  $\delta P(x)$  measured at 79 K for the light powers 1, 1/2, and 1/3 mW using an incident microwave power  $P_{\text{in}} = -8$  dBm and scaled to have the same peak amplitude.

3) where the YBCO film was much wider and less than half as thick. To emphasize changes in shape, the curves in Fig. 8 were scaled to have the same magnitude at the center of the strip. As  $T \rightarrow T_c$ , the measured  $\delta P(x)$  curves become narrower and the  $\delta P$  peaks also become narrower. This narrowing becomes more rapid as  $T \rightarrow T_c$ . As  $T$  is lowered the curves approach a low- $T$  limit shape. The same degree of narrowing of the  $\delta P(x)$  curves with increasing  $T$  is visible in Fig. 7, but is less obvious due to the much greater width of the microstrip. At first glance, this behavior suggests that changing the temperature alters the spatial distribution of the current. Care must be taken that the observed change is not due to the microwave power producing currents and fields that exceed critical values as the temperature rises. Care must also be taken that the magnitude of the local light-induced temperature rise is sufficiently small compared to the difference between the sample temperature and the critical temperature.

Several experiments were performed to address these concerns. Measurements of  $\delta P(x)$  at temperatures near  $T_c$  for lower incident microwave powers showed no measurable change in the shape of  $\delta P(x)$  so we conclude that current densities and fields exceeding critical values are not a concern in these measurements. A substantial effect on the shape of  $\delta P(x)$  was seen when the light power was reduced [see Fig. 8(b)]. At 79 K when the light power was reduced by a factor of 2,  $\delta P(x)$  resembled a curve measured at lower  $T$ . A further reduction in light power resulted in little further change in  $\delta P(x)$ . We observed that the closer  $T$  approached

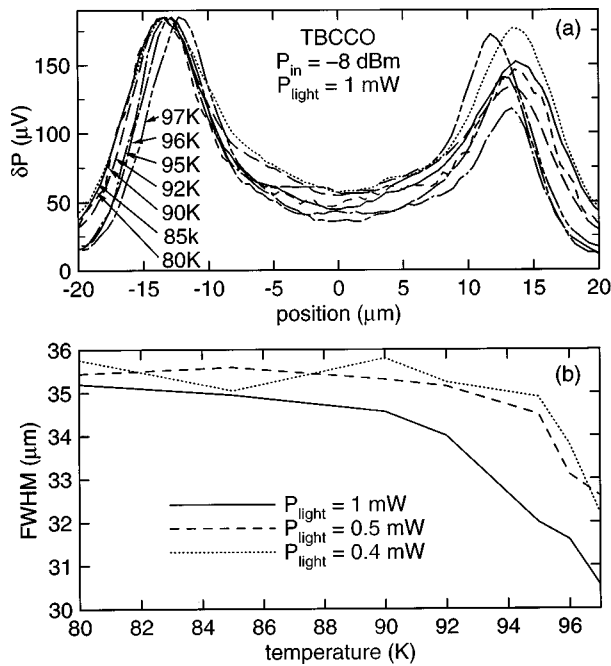


FIG. 9. Narrowing of photoresponse  $\delta P(x)$  for coplanar TBCCO sample 1 with increasing light power. (a)  $\delta P(x)$  measured for the temperatures 80, 85, 90, 92, 95, 96, and 97 K, and scaled to have the same magnitude for the left-hand edge-peak. Peak incident light power 1 mW. Incident microwave power  $P_{in} = -8$  dBm. As  $T \rightarrow T_c$ , the width of the measured  $\delta P(x)$  curves decreases. (b) Full width at half maximum of the  $\delta P(x)$  measurements plotted as a function of temperature for the light powers 1, 0.5, and 0.4 mW using an incident microwave power  $P_{in} = -8$  dBm. Because the left and right peaks differed in height, the half-maximum position for each side of the strip was determined using the magnitude of that side's edge-peak.

$T_c$  the more the light power had to be reduced for  $\delta P(x)$  to reach its low light power limit shape.

These observations clearly show that for temperatures approaching  $T_c$ , the light power must be reduced to avoid the act of measurement significantly altering the system being measured. If the  $\delta P(x)$  measurements in Fig. 8(a) were measured in the low power limit, then a larger range of peak-to-valley ratios would be seen (as in Fig. 7). All of the measurements of  $\delta P(x)$  discussed below for YBCO, except where explicitly mentioned, were performed using a light power low enough so that the act of measurement did not significantly alter the system being measured.

## 2. TBCCO kinetic-inductance photoresponse versus temperature and light power

A similar effect on  $\delta P(x)$  with changing the temperature is shown for the coplanar TBCCO sample (sample 1) in Fig. 9(a). Note that the curves in Fig. 9(a) were scaled to have the same magnitude at the left edge-peak. Each curve is the average of a dozen spatial scans (each scan being performed at a slightly different position along the strip spaced apart by several microns); this was done to remove the photoresponse contributions believed to be associated with intergranular regions. It is clear from Fig. 9(a) that this averaging has been only moderately successful. Nevertheless, the same decrease in the width of the  $\delta P(x)$  distribution with increasing  $T$  that was seen for YBCO is also seen for TBCCO.

Figure 9(b) is a plot of the widths (FWHMs) of the  $\delta P(x)$  curves as a function of  $T$  measured for the same light power used in Fig. 9(a) and two lower powers. The behavior of the photoresponse with light power for TBCCO is similar to that of YBCO with the added feature of pathologically sensitive local positions such as that observed in Fig. 5(c). The FWHM of a  $\delta P(x)$  curve should approximately equal the width of the strip (30  $\mu m$ ) plus an amount somewhat less than (due to the edge-peak asymmetry) the FWHM of the spatial resolution function ( $\sim 6.6$   $\mu m$ ).

Just as for YBCO, these observations clearly show that for temperatures near  $T_c$ , the light power must be reduced to avoid the act of measurement significantly altering the system being measured. All measurements of  $\delta P(x)$  shown below for TBCCO, except where explicitly mentioned, were performed using light powers low enough so that the act of measurement did not alter the system being measured.

The behavior of the photoresponse with light power that was noted above for YBCO is not specific to YBCO—it is observed for TBCCO as well. Any explanation put forward to explain one should explain the other.

## 3. YBCO resistive-transition photoresponse versus temperature and light power

In this section we consider resistive-bolometric photoresponse measurements (see Sec. II B) that were performed with the temperature in the resistive transition. Two YBCO samples were used—differing in film thickness and width. Recall that for the resistive-transition photoresponse we expect  $\delta P = -I^2 \delta R_D$  [Eq. (6)] where  $I$  is the current in the film underneath the light spot. For these measurements the microwave frequency was set far from any resonance and the light was scanned not across a part of the loop, but rather across the input transmission line.

Figure 10(a) shows a measurement of the transmitted microwave power  $P(T)$  as well as measurements of  $\delta P(x)$  that were performed at three different temperatures spanning the resistive transition. The  $\delta P(x)$  measurements shown in the inset at the lower left are scaled to have the same magnitude at  $x=0$ ; this was done to emphasize the observed changes in the shape of  $\delta P(x)$ . As the temperature increased, the measured  $\delta P$  edge-peaks became less prominent; the  $\delta P(x)$  distribution became flatter until, at the highest  $T$ , no edge-peaks were detected within the spatial resolution of our measurement. This behavior is consistent with the type of current redistribution expected with the increasing penetration of magnetic fields (see Fig. 7). The existence and qualitative behavior of the edge-peaks is evidence that the analysis in Sec. II B correctly relates the resistive-transition photoresponse to the current. This data suggests that a dramatic change in the shape of the spatial distribution of the current in the strip occurs as the temperature passes through the resistive transition.

For the kinetic-inductance photoresponse measurements, it was observed that this light power was sufficient to significantly perturb the system being measured. One observation that raises concern is that at all three temperatures, the width of  $\delta P(x)$  is significantly smaller than the physical width of the superconducting strip. The effect of reducing the light

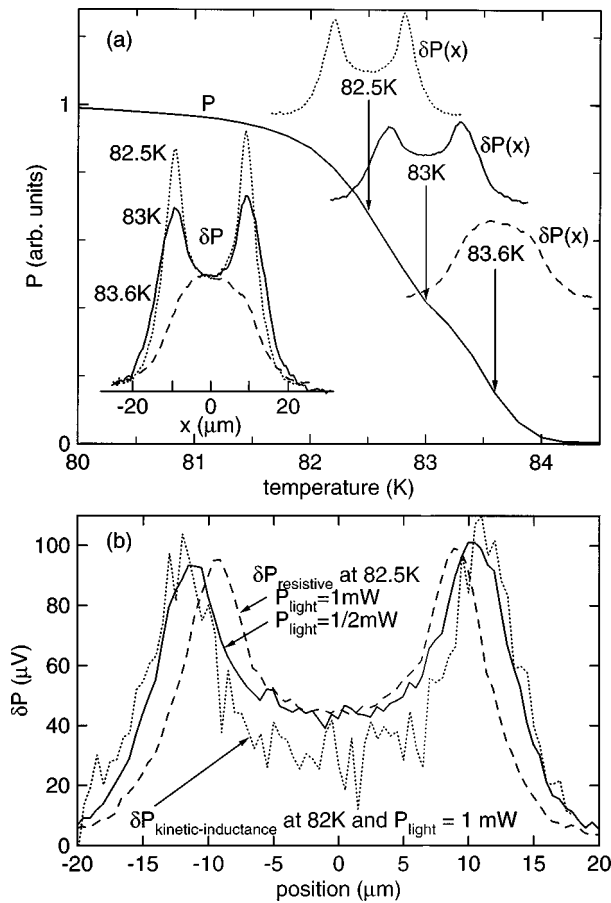


FIG. 10. (a) The resistive transition of the coplanar YBCO sample 2 and the resistive-transition bolometric photoresponse  $\delta P(x)$  measured at temperatures within the resistive transition. The incident light power was 1 mW and the incident microwave power was  $P_{\text{in}} = -8$  dBm. The microwave frequency was 1.75 GHz—far enough from any resonance frequency of the loop to make the presence of the loop inconsequential. A measurable  $\delta P(x)$  was observed when the light spot was scanned across the power input transmission line; no  $\delta P$  was observed on the loop. Photoresponse measurements performed at 82.5, 83, and 83.6 K are plotted both in the inset at lower left and above the temperatures at which they were measured. (b) Resistive-bolometric photoresponse  $\delta P_{\text{resistive}}$  measured at 82.5 K for light powers of 1 and 1/2 mW. Also shown for comparison is the kinetic-inductance photoresponse  $\delta P_{\text{kinetic-inductance}}$  measured at 82 K using a light power of 1 mW. All curves have been scaled to have approximately the same magnitude.  $(1\text{ mW } \delta P_{\text{resistive}}) \times 1$ ,  $(1/2\text{ mW } \delta P_{\text{resistive}}) \times 1.7$ , and  $(1\text{ mW } \delta P_{\text{kinetic-inductance}}) \times 23.5$ . The microwave power  $P_{\text{in}} = -8$  dBm was used for all measurements.

power on the measured  $\delta P(x)$  is shown in Fig. 10(b). The solid and dashed curves are resistive-transition  $\delta P(x)$  measurements performed at 82.5 K using the light powers 1 and 1/2 mW, respectively. This reduction of the light power by a factor of 2 increased the width of  $\delta P(x)$  by 4  $\mu\text{m}$ . This is the same qualitative behavior that was observed as  $T \rightarrow T_c$  for the kinetic-inductance photoresponse measurements. That two very different current-measuring photoresponse techniques yield the same behavior suggests that the current distribution is altered when probed using too much light power. To measure an unperturbed current distribution near  $T_c$ , the light power must be reduced until the shape of the current distribution no longer changes. Also plotted in Fig. 10(b), for purposes of comparison, is a kinetic-inductance  $\delta P(x)$  mea-

sured at a slightly lower temperature (82 K) using a light power of 1 mW.

In contrast to the resistive-transition measurements shown in Fig. 10, the resistive-transition  $\delta P(x)$  measurements in Figs. 11 and 12 were taken using the thinner (2000 Å thick) YBCO film (sample 3) used in Figs. 3 and 7. Measurements of the kinetic-inductance photoresponse for this sample show  $\delta P(x)$  flattening out as  $T \rightarrow T_c$  (see Fig. 7). The two-dimensional resistive-transition  $\delta P(x, y)$  measurement in Fig. 11 was taken at 87 K in the middle of the resistive transition and shows a photoresponse that, barring subtle edge peaks, is approximately flat across the width of the microstrip. These  $\delta P(x)$  curves were measured at 10  $\mu\text{m}$  intervals along the microstrip covering a total length of 0.29 mm and are offset vertically in the figure such that microwave power flows from the top curve toward the bottom curve. The irregularities observed along the microstrip are believed associated with local imperfections that were small enough to not affect the kinetic-inductance photoresponse measurements on this sample.

The data shown in Fig. 12 were measured at a position along the microstrip line corresponding to the top curve in Fig. 11—a position with no prominent film imperfections. The photoresponse was measured at seven temperatures—covering the full width of the resistive transition. The  $\delta P(x)$  curves are shown scaled to have the same amplitude and offset to illustrate the progression of shape changes. In this thin sample at these temperatures, the magnetic field penetration depth is much larger than the thickness of the film. This explains the much more subtle current peaks that are observed in Fig. 12 compared to Fig. 10.

#### D. The degree of perturbation: Estimates of local light-induced temperature rise

For any new measurement technique, it is important to establish the range of conditions for which the measurement is valid. With this motivation, in the following two sections, we estimate the magnitude of the local temperature modulation  $\delta T_{\text{local}}$  that is created by the absorption of a focused 1 mW light beam whose intensity is modulated at  $f_{\text{light-chop}} \sim 1/2$  MHz.

Before addressing the absolute magnitude of  $\delta T_{\text{local}}$  we must first consider a separate issue of equal importance: Does the magnitude of the light induced temperature rise  $\delta T_{\text{local}}$  depend on the location of the light spot relative to the edge of the superconducting strip? This concern arises, because heat diffuses laterally as well as into the substrate; near the center of a superconducting strip, heat can diffuse laterally in all directions within the plane of the superconductor; near the edge of the strip, it cannot. This suggests that the magnitude of the temperature modulation is larger when the light spot is within a diffusion length of the strip's edges. To address this concern we measured  $\delta P(x)$  for different  $f_{\text{light-chop}}$ . For YBCO at temperatures below where light-power effects on the shape of  $\delta P(x)$  were appreciable, the spatial resolution of the  $\delta P(x)$  measurements increased with increasing  $f_{\text{light-chop}}$  until  $f_{\text{light-chop}} \sim 1/3$  MHz. Above this frequency the spatial resolution of the  $\delta P(x)$  measurements did not measurably improve and it is presumed that the thermal

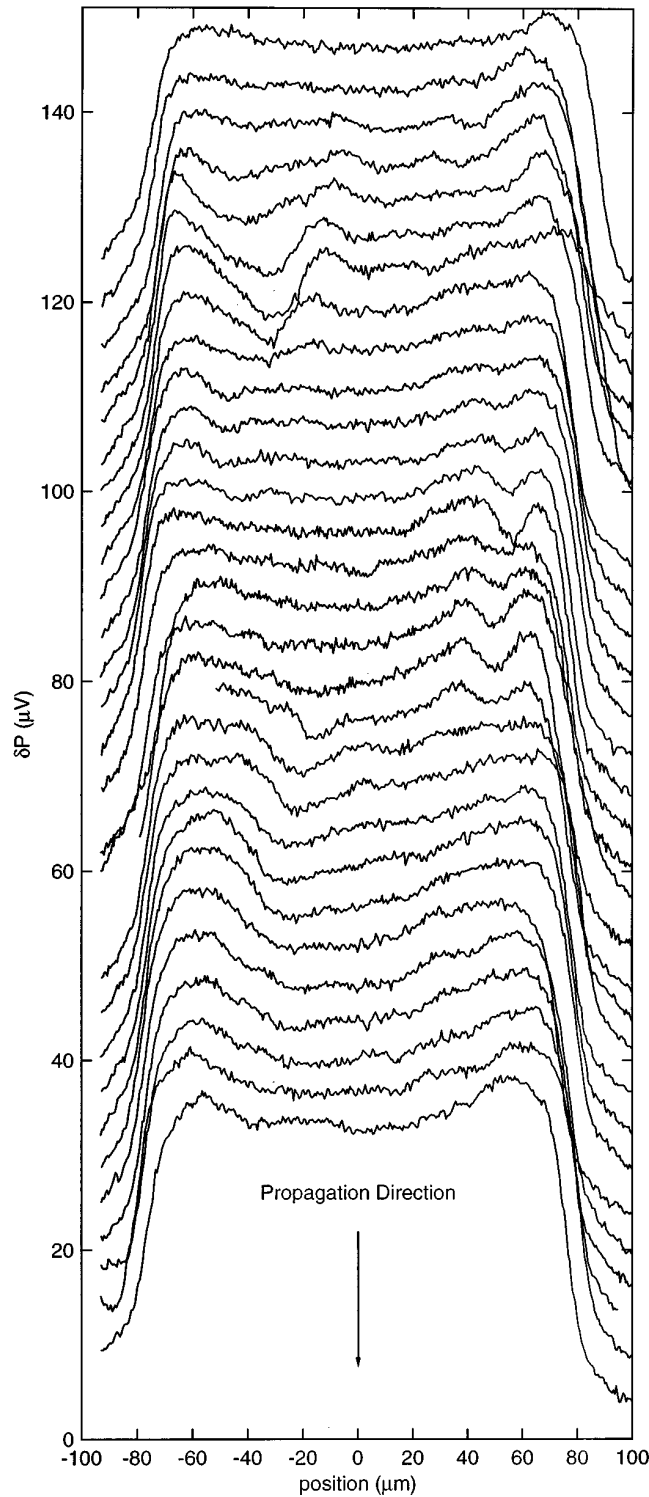


FIG. 11. Two-dimensional resistive-transition photoresponse  $\delta P(x,y)$  measurement on a 2000 Å thick YBCO microstrip transmission line (sample 3). Between each  $\delta P(x)$  measurement across the 150  $\mu\text{m}$  wide strip the light scan path was translated 10  $\mu\text{m}$  in the  $y$  direction along the transmission line. The total distance between the top trace and the bottom trace corresponds to a distance of 0.29 mm along the transmission line. All measurements were performed at 87 K (in the middle of the resistive transition). A microwave frequency of 3.4 GHz was used—far from any resonance of the structure. The incident microwave power was  $-22$  dBm.

diffusion length became small compared to the size of the light spot so that only a small part of the illuminated material was affected by the presence of the edge. That a stable high  $f_{\text{light-chop}}$  limit shape for  $\delta P(x)$  was measured means that

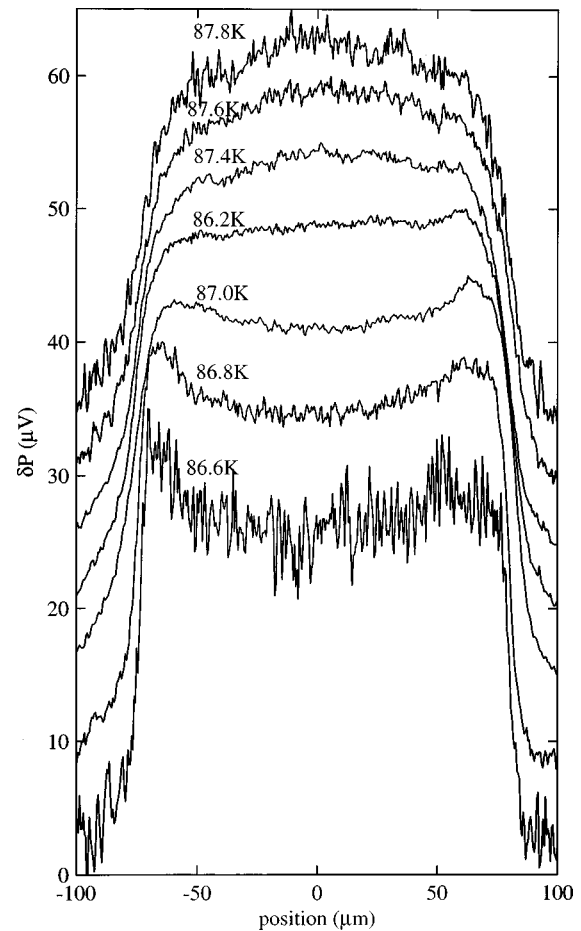


FIG. 12. Resistive-transition photoresponse  $\delta P(x)$  measurements made on a 150  $\mu\text{m}$  wide microstrip transmission line patterned from a 2000 Å thick film of YBCO (sample 3). This figure shows seven  $\delta P(x)$  curves, measured for various temperatures covering the full width of the resistive transition. To emphasize shape changes the  $\delta P(x)$  curves have been scaled to have the same amplitude as the largest curve (87 K). The curves have been offset vertically to illustrate the progression of shape changes. In this thin sample at these temperatures, the magnetic field penetration depth is much larger than the thickness of the film.

either (1) there is negligible contribution from the region having an enhanced  $\delta T_{\text{local}}$  because that enhancement occurs in only a small fractional volume of the entire illuminated region (even though the largest contributions to  $\delta P$  come from the edge) or (2) there is no significant enhanced  $\delta T_{\text{local}}$  (This could happen because the thermal diffusion length for the substrate is at least an order of magnitude larger than that of the film and heat reaching the film/substrate interface gets efficiently conducted away into the substrate). Either way, we conclude that it is valid to speak of a light-induced temperature rise—independent of the position of the light spot relative to the strip edge.

Clear evidence that the light induced temperature rise  $\delta T_{\text{local}}$  changes with the distance of the light spot from the edge of the film comes from observations of the phase lag of  $\delta P$  behind the light source. Changes in phase lag are caused by changes in the thermal time constant for heat transport out of the film. Changes in the thermal time constant result in changes in  $\delta T_{\text{local}}$ . The phase lags of both kinetic-inductance

and resistive-transition photoresponses varied symmetrically about the strip center—with most of the change occurring near the strip edges. From our phase lag observations and a simple heat transport model, we estimate that variation in  $\delta T_{\text{local}}$  across the strip is negligible.

### 1. $\delta T$ from resistive-transition photoresponse

The light-induced temperature rise  $\delta T_{\text{local}}$  of the illuminated part of the transmission line can be determined from measurements of  $\delta P$  and  $P$  made while scanning the temperature through the resistive transition. The relation that connects  $\delta P$  to a temperature rise  $\delta T$  of the *whole* transmission line is  $\delta P = \partial P / \partial T \delta T$ . If only a fraction  $1/N$  of the length of the strip is illuminated and heated up by  $\delta T_{\text{local}}$ , then the light-induced change in transmitted microwave power  $\delta P$  is a factor of  $1/N$  smaller.<sup>27</sup> If only part of the strip's width is illuminated, then  $\delta P$  will be smaller by the fraction of  $[\int J^2(x) dx]_{\text{under-light-spot}} / [\int J^2(x) dx]_{\text{across-strip}}$  [see Eq. (6)]. For the YBCO coplanar sample 2, the local temperature increase was calculated to be  $\delta T_{\text{local}} \sim 1$  K for a 1 mW light beam modulated at  $\sim 0.4$  MHz and focused to a FWHM  $\sim 6.6$   $\mu\text{m}$  spot. To accurately characterize the current distribution within the resistive transition it is necessary to reduce the light power until  $\delta T_{\text{local}}$  small compared to the several degree width of the superconducting transition. The local temperature rise calculated for TBCCO was not significantly different.

### 2. $\delta T$ from kinetic-inductance photoresponse

A kinetic-inductance photoresponse is acquired by setting the microwave frequency to be on the shoulder of a resonance and measuring the change in the transmitted microwave power that occurs as the absorption of light shifts the frequency of the resonance. The magnitude of this photoresponse [from Eq. (1)] is  $\delta P = (\partial P / \partial f) \delta f$ , where  $\delta f$  is the light-induced shift in the resonant frequency. If  $\delta f$  occurred because the temperature of the entire resonant structure was increased by  $\delta T$ , then we would have  $\delta f = (\partial f / \partial T) \delta T$ , where  $\partial f / \partial T$  was determined from the measurement of  $f(T)$ , the resonance frequency as a function of temperature. To determine the *local* temperature rise  $\delta T_{\text{local}}$  caused by focusing a light beam onto the superconductor some additional considerations are necessary.

To determine the effect of a local temperature rise, consider that if the temperature of the entire structure is raised by  $\delta T$ , the contribution that each part of the structure makes to  $\delta f$  is proportional to the local value of  $J^2$  [see Eq. (5)]. For equal temperature rises, the frequency shift  $\delta f_{\text{local}}$  due to local heating is thus related to the frequency shift  $\delta f$  due to global heating by

$$\frac{\delta f_{\text{local}}}{\delta f} = \frac{[\int J(x', y', z')^2 dx' dy' dz']_{\text{light-spot}}}{[\int J(x', y', z')^2 dx' dy' dz']_{\text{everywhere}}}, \quad (7)$$

where the integral in the denominator is over the entire superconductor volume of the resonant structure including the current in the ground planes.

To get the same shift of the resonance frequency from heating a local spot that occurs from heating the whole struc-

ture, the local temperature rise  $\delta T_{\text{local}}$  must be larger than  $\delta T$  by a factor given by  $\delta T_{\text{local}} / \delta T = \delta f / \delta f_{\text{local}}$ . The local temperature rise  $\delta T_{\text{local}}$  can be determined using this relationship, Eqs. (1) and (7), and the measurements of  $\delta P(f)$ ,  $P(f)$ , and  $f(T)$ .

For the YBCO coplanar transmission line sample 2 studied here illuminated by a 1 mW light beam modulated at  $\sim 0.4$  MHz and having a FWHM  $\sim 6.6$   $\mu\text{m}$ , the temperature rise is estimated to be  $\delta T_{\text{local}} = 1.4 \pm 0.2$  K at 81 K. No systematic variation in  $\delta T_{\text{local}}$  was observed for  $T$  between 74 K and 81 K. The temperature rise calculated for TBCCO was not significantly different.

There is good agreement between the local temperature rise calculated using the resistive-transition photoresponse and the local temperature rise calculated using the kinetic-inductance photoresponse. For  $T$  well below  $T_c$  where a local temperature rise  $\Delta T_{\text{local}} \sim 1$  K results in  $\Delta \lambda / \lambda \ll 1$  the act of measurement should not significantly alter the system being measured. As  $T \rightarrow T_c$  this same  $\Delta T_{\text{local}}$  can result in a significant change in  $\Delta \lambda / \lambda$  and care must be exercised in the interpretation of  $\delta P$ .

## VI. HIGH MICROWAVE POWER BEHAVIOR

In this section we examine the effect that high microwave currents and their associated fields have on the spatial distribution of current in high-temperature superconducting films. As the current is increased, deviations in the shape of the current distribution are expected to occur first at the edges of the superconducting strip where the current densities and their associated fields are largest. All measurements were performed at temperatures and light powers low enough so that the probing light spot did not significantly perturb the system being measured.

High microwave powers were achieved not by using a high power source, but rather by performing measurements on resonant structures driven by a more modest microwave source. The power amplification inside the resonant structure was calculated using a simple lumped element model. The microwave power at the peak of the standing wave in the resonant loop  $P_{\text{peak}}$  can be expressed in terms of the incident power  $P_{\text{in}}$ , and the position, depth, and width of the resonance. The peak microwave power  $P_{\text{peak}}$  was calculated at the frequency on the shoulder of the resonance where the transmitted microwave power changes most rapidly with frequency—the inflection point. This choice of microwave frequency corresponds to the conditions for which the kinetic-inductance photoresponse measurements reported in this work were performed. The ratio of  $P_{\text{peak}}$  at the inflection point to the incident microwave power  $P_{\text{in}}$  is

$$\frac{P_{\text{peak}}}{P_{\text{in}}} = \frac{4}{\pi} \left( \frac{f_0}{\Delta f} \right) \times \left( \frac{S_{\Delta f}^2 - S_0^2}{1 - S_{\Delta f}^2} \right)^{1/2} \frac{1 - S_0}{1 + \frac{S_0^2}{3} \left[ \left( 1 + \frac{3}{S_0^2} \right)^{1/2} - 1 \right]}, \quad (8)$$

where  $f_0$  is the center frequency of the resonance. The fractional depth of the resonance  $S_0 (< 1)$  is the ratio of the

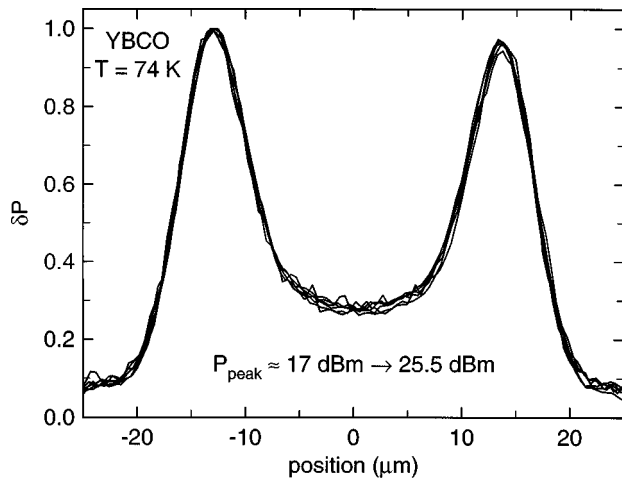


FIG. 13. Plot of the measured photoresponse  $\delta P(x)$  across the 30 mm wide YBCO coplanar transmission line (sample 2) for six different peak microwave powers ( $P_{\text{peak}} = +17.0, +20.8, 22.6, 23.7, 24.3$ , and  $25.5$  dBm). All measurements were performed at 74 K using an incident light power of 1 mW. The resonance line shape  $\delta P(f)$  was measured for each microwave power so the peak microwave power could be calculated. Of the two first-harmonic resonances, the one corresponding to the higher frequency was used. No systematic change in the spatial profile  $\delta P(x)$  was detected.

transmitted amplitude at the center of the resonance to the transmitted amplitude measured off resonance. The full width  $\Delta f$  of the resonance was measured between the points at which the transmitted amplitude had dropped by  $S_{\Delta f}$  relative to the off-resonance transmission. In most cases  $\Delta f$  was measured at the 3 dB points where  $S_{\Delta f}^2 \approx 1/2$ . All incident and peak powers are time-averaged powers. The peak time averaged power is related to the peak spatial and temporal total current  $I$  flowing along the strip by

$$P_{\text{peak}} = \frac{1}{2} I^2 Z_c, \quad (9)$$

where  $Z_c \approx 50 \Omega$  is the characteristic impedance of the coplanar transmission line. The peak current in the superconducting strip can be determined for any given incident microwave power using Eqs. (8) and (9). The peak current density is determined from the peak current passing through a cross section of the transmission line and the knowledge of the shape of the current distribution on that cross section. The transverse distribution of current on the superconducting strip is extracted from our  $\delta P(x)$  measurements. The current distribution through the depth of film is estimated from the solution of a superconducting plane sandwiched between antiparallel magnetic fields.

### A. YBCO at high microwave powers

The photoresponse  $\delta P(x)$  measured by scanning a focused light beam across the 30  $\mu\text{m}$  wide YBCO coplanar strip line is shown in Fig. 13 for six different microwave powers. Over this power range, Wilker *et al.*<sup>5</sup> observed that for YBCO the power in the third harmonic of the applied power increased as the cube of the applied power—whereas for TBCCO it increased more slowly than cubic. To emphasize changes in shape, the measurements in Fig. 13 were scaled to have the same amplitude. These measurements were performed at a position on the resonant loop corre-

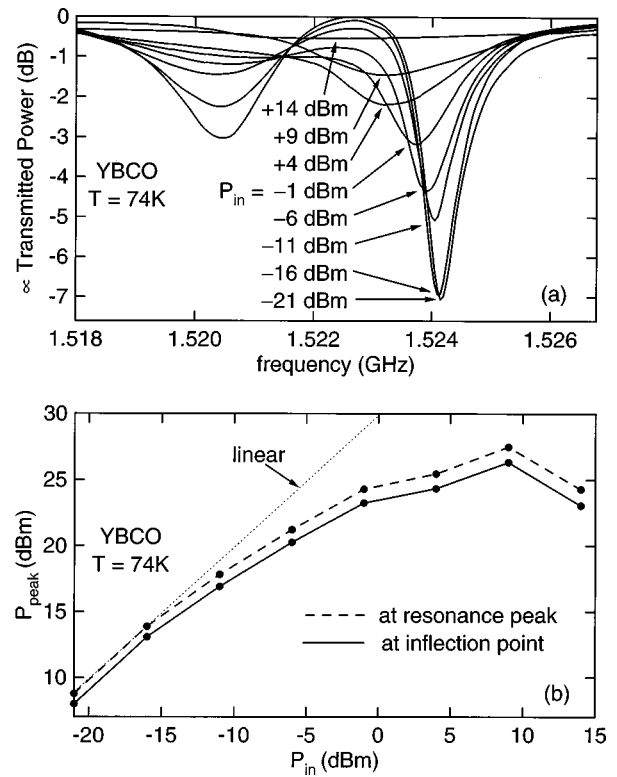


FIG. 14. (a) Fundamental resonances of the YBCO coplanar resonator (sample 2) measured as a function of microwave power at 74 K. The incident powers  $P_{\text{in}}$  used for the measurements are indicated on the figure. (b) Calculated spatial peak microwave powers  $P_{\text{peak}}$  within the loop for the resonances shown in (a) plotted in as a function of  $P_{\text{in}}$ . The solid line is the  $P_{\text{peak}}$  calculated for the microwave frequency set at the inflection point of the upper resonance where  $\partial P/\partial f$  is at maximum. This corresponds to the conditions used in the  $\delta P(x)$  measurements. The dashed line is  $P_{\text{peak}}$  calculated for the microwave frequency set at the center frequency of the upper resonance. The incident microwave power was varied from the linear regime until the resonance was fully saturated.

sponding to a peak in the standing wave. All measurements were performed at 74 K. The shape of the resonance  $P(f)$  was measured for each microwave power so that [using Eq. (8)] the peak microwave power could be calculated.

Within the noise of the measurements, the shape of the spatial profiles of the photoresponse  $\delta P(x)$  did not change with microwave power. The average width of the superconducting strip extracted from fits to  $\delta P(x)$  was  $29.8 \pm 0.3 \mu\text{m}$ . The 30  $\mu\text{m}$  physical width of the superconducting strip lies within these error bars. It was observed in Fig. 8 that if the light power is too high, the probing light beam can alter the system being measured in such a way that the  $\delta P(x)$  spatial profile becomes narrower. The agreement between the physical width and the measured width of the strip is evidence that the light power used in these measurements is sufficiently low.

The peak microwave powers  $P_{\text{peak}}$  achieved within the resonant loop are as large as can be achieved at 74 K. This can be seen from Fig. 14(b), which shows that the calculated  $P_{\text{peak}}$  within the resonator saturates with increasing input power  $P_{\text{in}}$ . Figure 14(a) shows the eight  $P(f)$  measurements of the first harmonic resonances that were used to calculate the  $P_{\text{peak}}(P_{\text{in}})$  curves shown in Fig. 14(b); the time

averaged incident powers  $P_{in}$  used for the measurements in part (a) are indicated on the figure. The input microwave power used in these measurements covered a range of 35 dB over which the  $P_{peak}(P_{in})$  function varied from linear to fully saturated. The solid line in Fig. 14(b) shows the  $P_{peak}$  reached in the loop when the microwave frequency is set at the inflection point where  $\partial P/\partial f$  is at maximum. This corresponds to the conditions used in the  $\delta P(x)$  measurements. The dashed line shows the  $P_{peak}$  reached in the loop when the microwave frequency is set at the center frequency of the resonance.

The lack of a change in the shape of  $\delta P(x)$  for YBCO over this range of microwave powers is consistent with third-harmonic generation measurements performed by Wilker *et al.*<sup>5</sup> They applied a power  $P_1$  to a coplanar transmission line and measured the power  $P_3$  generated in the third harmonic of the applied microwave frequency. They observed that the third-harmonic generation was well characterized by  $P_3 \propto P_1^3$  for a range of powers that covers those used in this work. This behavior is expected, because we observed no change in the spatial profile of the current (and thus field) distributions within the superconducting film. Presumably, it is the peak current at the edge of the strip that is responsible for the nonlinearities that generate power in the third harmonic of the applied frequency.

The magnitude of the peak current density in the superconductor can be established using measurements of the resonance  $P(f)$ , Eqs. (8) and (9), and the current distribution inferred from measurements of the spatial profile of the photoresponse  $\delta P(x)$ . The highest power used in Fig. 14(a) corresponds to a peak power of  $P_{peak} \approx 25.5$  dBm or 0.36 W. Using Eq. (9) this implies a current  $I = [2 \times 0.36 \text{ W} / 50 \Omega]^{1/2} = 0.12$  A flows through the  $30 \mu\text{m}$  wide by  $0.45 \mu\text{m}$  thick cross section of the strip at the peak of the standing wave. The average current density is thus  $\langle J \rangle = 8.9 \times 10^5 \text{ A/cm}^2$ . From fits to the photoresponse  $\delta P(x)$ , the  $J(x)$  distribution is found to have a peak-to-average ratio  $J_{edge-peak}/\langle J \rangle = 3.3$ . Finally we estimate a 2:1 peak-to-average ratio for the current distribution through the thickness of the film. This implies a peak spatial and temporal current density for the highest microwave power used at 74 K of  $J_{edge-peak} \approx 5 \times 10^6 \text{ A/cm}^2$ . This current density corresponds to a surface magnetic field below  $H_{c1}$  for YBCO at 74 K.

## B. TBCCO at high microwave powers

The photoresponse  $\delta P(x)$  measured by scanning a focused light beam across a  $30 \mu\text{m}$  wide TBCCO coplanar line is shown in Fig. 15(a) for twelve different microwave powers. For this power range, Wilker *et al.*<sup>5</sup> observed that for TBCCO the power in the third harmonic of the applied power increased more slowly than the cube of the applied power—whereas for YBCO it increased as the cube. To emphasize changes in shape, these measurements in Fig. 15(a) are scaled to have the same amplitude. Each  $\delta P(x)$  curve shown is the average of about ten  $\delta P(x)$  measurements—each measurement was performed with the light spot scanned across a slightly different position along the copla-

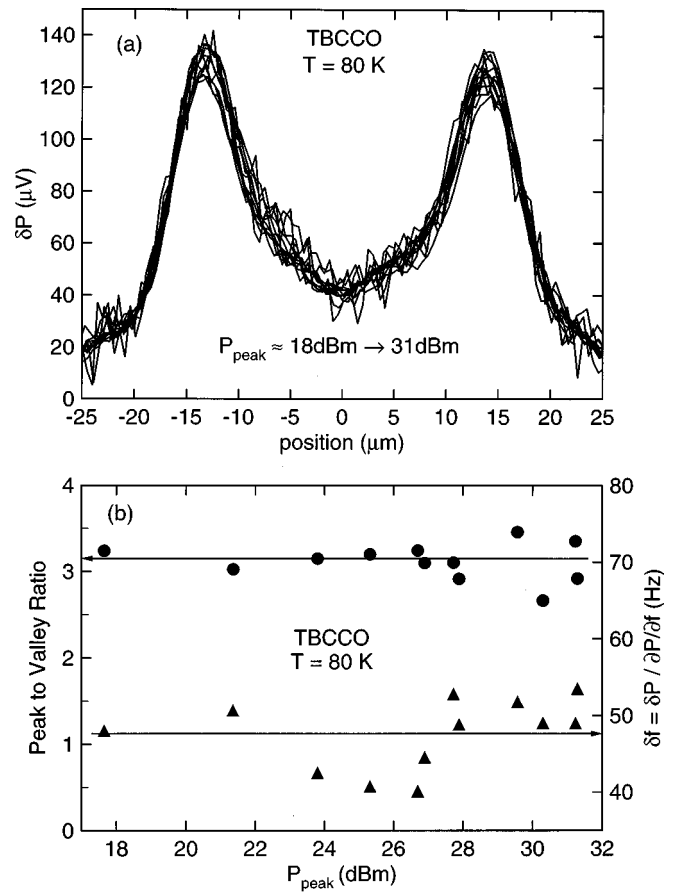


FIG. 15. Effect of microwave power on photoresponse  $\delta P(x)$  measured on the coplanar TBCCO transmission line (sample 1). Of the two first-harmonic resonances, the one having the lowest frequency was used to measure  $\delta P(x)$ . (a)  $\delta P(x)$  measured for twelve different peak microwave powers  $P_{peak}$  ranging from  $\sim 18$  to  $\sim 31$  dBm. Each curve is an average of about ten  $\delta P(x)$  measurements; between each individual  $\delta P(x)$  measurement, the path of the light spot was translated several microns along the strip. These curves were averaged to remove the granular contribution to the photoresponse. (b) Plotted as  $\bullet$ 's is the ratio of the peak photoresponse measured at the strip edge to that measured at the strip center plotted as a function of  $P_{peak}$ . This peak-to-valley ratio is constant within the accuracy of the measurement. Plotted as  $\blacktriangle$ 's is the light-induced frequency shift  $\delta f$  of the resonance as a function of  $P_{peak}$ .

nar strip (spaced apart by several microns). This was done to average out the contributions to the photoresponse that are believed due to the intergranular regions. All measurements were performed at positions on the resonant loop indistinguishable from the peak of the standing wave. All measurements were performed at 80 K. The peak power of the probing light beam incident on the sample was 1 mW. The shape of the resonance  $P(f)$  was measured for each microwave power so that with the aid of Eq. (8) the peak microwave power could be calculated.

Within the noise of the measurements, the shape of the spatial profiles of the photoresponse  $\delta P(x)$  did not change with microwave power. The peak-to-valley ratio for the photoresponse, plotted as  $\bullet$ 's in Fig. 15(b), is constant, unchanging with power. The width of the superconducting strip as measured from the FWHM of  $\delta P(x)$  was also constant.

Within the noise of the measurements, the light-induced frequency shift  $\delta f = \delta P / (\partial P / \partial f)$  of the resonance did not



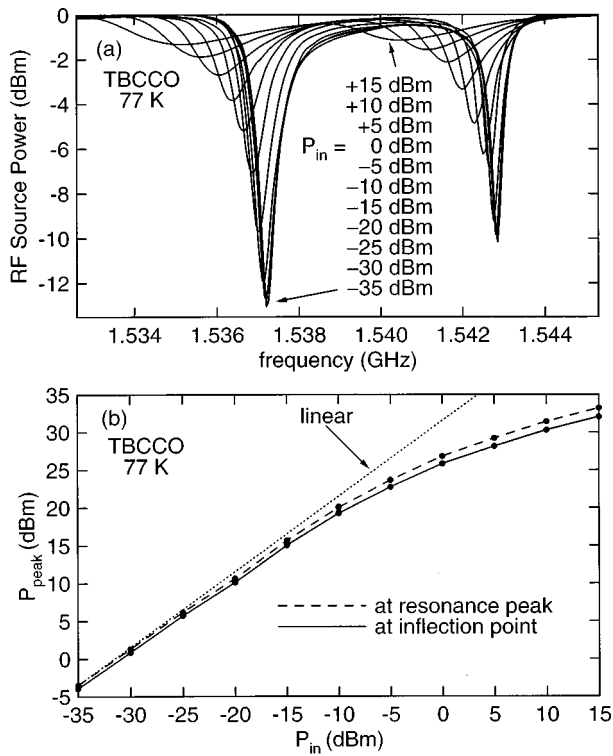


FIG. 16. (a) Fundamental resonances of the TBCCO coplanar resonator (sample 1) measured as a function of microwave power at 77 K. The incident powers  $P_{in}$  used for the measurements are indicated on the figure. (b) Peak spatial powers calculated from incident microwave powers and the positions and shapes of resonances shown in (a). The dashed line is  $P_{peak}$  calculated for the microwave frequency set at the center of the lower resonance. The solid line is  $P_{peak}$  calculated for the microwave frequency set at an inflection point of the lower resonance. The straight dotted line shows a linear power relation. As  $P_{in}$  was increased,  $P_{peak}$  changed from increasing linearly with  $P_{in}$  to almost the point of saturation. Powers for 80 K fell  $\sim 1$  dB below those plotted here for 77 K.

change with microwave power [see  $\blacktriangle$ 's in Fig. 15(b)]. These frequency shifts were calculated using the  $\delta P$  measurements in Fig. 15(a) for which the presumed granular contribution to the photoresponse has been averaged out. If an increase in  $\delta f$  had been observed with increasing  $P_{peak}$ , this would indicate that higher microwave powers were enhancing the light-induced penetration of magnetic fields into the superconductor.

The peak microwave powers  $P_{peak}$  achieved within the resonant loop are *almost* as large as can be achieved at 80 K. This is illustrated for 77 K in Fig. 16(b), which shows  $P_{peak}$  within the resonator approaching saturation with increasing input power  $P_{in}$ . Figure 16(a) shows the eleven  $P(f)$  measurements of the first harmonic resonances that were used to calculate the  $P_{peak}(P_{in})$  curves shown in Fig. 16(b); the incident powers  $P_{in}$  used for the measurements in Fig. 16(a) are indicated on the figure. The input microwave power used in these measurements covered a range of 50 dB over which the  $P_{peak}(P_{in})$  function varied from linear to almost saturated. The solid line in Fig. 16(b) shows the  $P_{peak}$  reached in the loop when the microwave frequency is set at the inflection point where  $\partial P/\partial f$  is at maximum. This corresponds to the conditions used in  $\delta P(x)$  measurements. The dashed line shows the  $P_{peak}$  reached in the loop when the microwave

frequency is set at the center frequency of the resonance.

That  $\delta P(x)$  doesn't change shape with increasing microwave power [see Fig. 15(a)] for the TBCCO film is a significant result. Over this same range of microwave powers Wilker *et al.*<sup>5</sup> observed an anomalously low third-harmonic generation rate for TBCCO films. We observed no change with power of the spatial profile of the intrinsic current and field distributions. Such changes in the current distribution would affect the generation of power at higher harmonics by the nonlinearities of the system. Deviations of third-harmonic power generation from  $P_3 \propto P_1^3$  can occur either through redistribution of current or through the nature of the nonlinear mechanism itself changing. Given these observations, it is natural to look for extrinsic or morphological origins for the nonlinearities that give rise to the generation of third-harmonic power. In Fig. 15(a) the extrinsic  $\delta P(x)$  photoresponse observed in the TBCCO sample 1 was purposely averaged out so attention could be focused on intrinsic mechanisms. As seen in Fig. 5, large variations (believed associated with the granular nature of the TBCCO film) are seen in the measurements of  $\delta P(x)$ . Perhaps the answer to the weaker third-harmonic generation observed by Wilker *et al.* lies in the behavior of nonlinear processes that occur within intergranular regions.

The magnitude of the peak current density in the superconductor can be established using measurements of the resonance  $P(f)$ , Eqs. (8) and (9), and the current distribution inferred from measurements of the spatial profile of the photoresponse  $\delta P(x)$ . The highest power used in Fig. 15(a) corresponds to a peak power of  $P_{peak} \approx 31$  dBm or 1.26 W. Using Eq. (9) this implies a current  $I = [2 \times 1.26 \text{ W} / 50 \Omega]^{1/2} = 0.22$  A flows through the  $30 \mu\text{m}$  wide by  $0.65 \mu\text{m}$  thick cross section of the strip at the peak of the standing wave. The average current density is thus  $\langle J \rangle = 1.2 \times 10^6 \text{ A/cm}^2$ . From fits to the photoresponse  $\delta P(x)$  the  $J(x)$  distribution is found to have a peak-to-average ratio  $J_{edge-peak}/\langle J \rangle = 2.6$ . Finally we estimate a 2:1 peak-to-average ratio for the current distribution through the thickness of the film. This implies a peak spatial and temporal current density for the highest microwave power used at 80 K of  $J_{edge-peak} \approx 7 \times 10^6 \text{ A/cm}^2$ . This current density corresponds to a surface magnetic field higher than  $H_{c1}$  for this TBCCO at 80 K. The current density at the center of the strip for the lowest power measurement included in Fig. 15(a) corresponds to a surface magnetic field approximately equal to  $H_{c1}$ .

## VII. DISCUSSION

### A. Implications for models of high microwave power behavior and third-harmonic generation

Models for the behavior of the YBCO and TBCCO high-temperature superconductors at high microwave powers must explain not only the photoresponse observations reported here, but also the observed generation rate of power at the third harmonic observed by Wilker *et al.*<sup>5</sup> The coplanar test samples used in this work were also used to measure the harmonic generation. Measurements on the YBCO film showed  $P_3 \propto P_1^3$  (as expected for films of high quality and

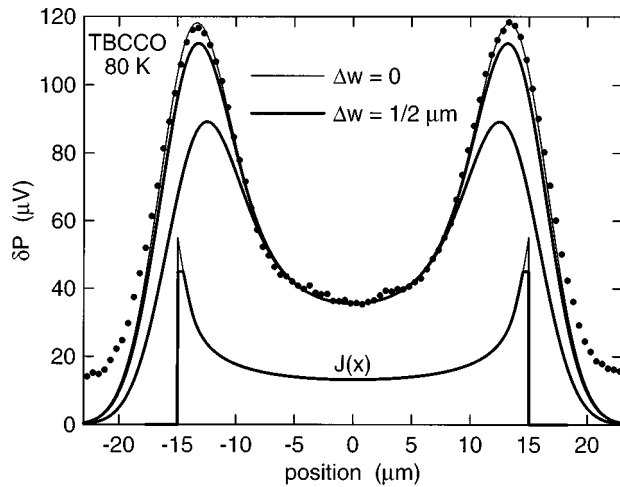


FIG. 17. Effect of spatially constant current wings on the shape of the photoresponse  $\delta P(x)$ . Plotted using dots is  $\delta P(x)$  measured across the coplanar TBCCO strip (sample 1) at 80 K with an incident microwave power of  $-9$  dBm. This data is an average of a dozen spatial scans measured at positions several microns apart along the strip. This was done to remove the photoresponse features believed associated with grain boundaries. The thin solid line through the data is the result of a fit that yielded the peaked current distribution shown at the bottom. A second current distribution, having a constant current density within  $\Delta w = 1/2 \mu\text{m}$  of the strip edge, is plotted below as a thick line. The thick lines passing through the  $\delta P(x)$  data are calculations of the photoresponse from the truncated current distribution—differing only in the treatment of the photoresponse coming from the truncated current region.

low defect density that are driven by fields below  $H_{c1}$ ). In contrast, measurements on the TBCCO film showed a slower growth of the third harmonic over the same range of applied microwave powers (for which  $H_{c1}$  was exceeded). If the mechanism for generating power in the third harmonic is intrinsic, then the rate at which power is generated in the third harmonic should depend on the shape of the spatial profile of the current distribution and not on film imperfections. Given this observation and the measured behavior of third-harmonic power generation in the YBCO and TBCCO samples, we expect to observe no change in the shape of the current distribution for YBCO and a substantial change in the shape of the current distribution for TBCCO. As no change in the intrinsic shape of  $\delta P(x)$  was observed with increasing microwave power for either type of film, only two possible conclusions can be made: (1) The measurement had insufficient sensitivity or resolution to observe the changes in the current distribution; or (2) The intrinsic current distribution did not change and the origin of the third-harmonic generation is extrinsic in nature.

It is important to establish how sensitive the  $\delta P(x)$  measurements reported here are to changes in the shape of the current distribution. Solely for the purpose of illustration, we consider the effects on  $\delta P(x)$  that result from current distributions predicted by the critical state model.<sup>28</sup> It is normally at the strip edges that the current density is largest and changes most rapidly with position. Consider the situation where the current density near the strip edge reaches the maximum current density  $J_{\text{max}}$  that the superconducting film can sustain. There should now be regions of constant current density  $J_{\text{max}}$ . The  $J(x)$  curve plotted with the wider line in

the bottom of Fig. 17 shows just such a situation. This curve shows a  $J(x)$  distribution with a  $1/2 \mu\text{m}$  wide region where  $J = J_{\text{max}}$  at the film edges. On top of it, plotted using a thinner line, is a  $J(x)$  distribution that has not been chopped off at  $J_{\text{max}}$ . This latter  $J(x)$  was extracted from the  $\delta P(x)$  data (dots) shown on this figure. The thin line through the data is the fit that was used to determine this  $J(x)$ . Two wider lines are plotted through the data. Both of these  $\delta P(x)$  curves were calculated from the truncated current distribution. The upper curve is a convolution of the square of the truncated  $J(x)$  curve with a Gaussian representing the spatial resolution of the measurement. This interpretation may exaggerate the contribution from the  $J = J_{\text{max}}$  regions. When the light probe modulates the temperature of a spot on the superconductor where  $J = J_{\text{max}}$ , neither the current density nor the magnetic fields in this region change—except through the temperature dependence of  $J_{\text{max}}$ . The lower thick line through the data in Fig. 17 shows the  $\delta P(x)$  that results from neglecting any contributions to  $\delta P$  from the region where  $J = J_{\text{max}}$ . Regardless of which treatment better reflects reality, it is clear that a  $1/2 \mu\text{m}$  wide region in which  $J_{\text{max}}$  has been reached produces as substantial change in the shape of the expected curve  $\delta P(x)$ .

An additional concern at high microwave powers is that the absorption of light could cause an increase in the local dissipation of microwave power. This added dissipation would cause an increase in  $\delta T_{\text{local}}$ . If a light-induced increase in the dissipation of microwave power is important, it is reasonable to expect that larger amplifications of  $\delta T_{\text{local}}$  should be observed at higher microwave powers. Calculating  $\delta T_{\text{local}}$  from measurements for a wide range of microwave powers can check this. Within experimental error, we find that  $\delta T_{\text{local}}$  is independent of microwave power. Another test of the microwave heating hypothesis is to look at the shape  $\delta P(x)$  measured across the superconducting strip. The microwave current density varies dramatically across the width of the strip. If microwave heating is important then it is reasonable to expect  $\delta T_{\text{local}}$  to be larger where the current density is larger. A  $\delta T_{\text{local}}$  that is dependent the local current density (and thus on position) would of necessity result in different shapes for  $\delta P(x)$  measured using different microwave powers. That we see no shape changes with microwave power suggests that light absorption enhancement of microwave heating is not important.

## B. Application of kinetic-inductance photoresponse to improve film growth and device performance

The kinetic-inductance photoresponse technique is amenable to characterizing the local microwave transport characteristics of unpatterned superconducting films. As such, it can be a valuable aid in growth efforts to improve film quality for microwave applications. In this variation of our technique, an unpatterned film serves as one wall of a microwave cavity. A light beam is focused through the optical quality transparent substrate onto the “underside” of the superconducting film. Cavity resonator systems have much higher  $Q$ 's than the transmission line resonators used in this work (due primarily to their lower volume to surface ratio). The sharper resonance yields a much higher sensitivity. This high sensi-

tivity enables two-dimensional raster scanning of a low power focused light beam over a surface to be done in a reasonable time at spatial resolutions of  $\sim 10 \mu\text{m}$ . The current distribution of the cavity modes should be clearly seen. The quantity and nature of the local deviations in the current distribution on unpatterned films could be studied for a variety of growth parameters. The growth parameters could then be varied to minimize the presence of these microwave detected film defects.

The association of local defects observed with this photoresponse technique to pertinent microwave characteristics in actual devices could be of great value. This association can be built in the following manner: The behavior of local deviations of the current distribution would first be studied and characterized by their differing behaviors as functions of temperature, microwave power, and light power. Devices would then be fabricated including and excluding these defective regions. Studying the difference in the behavior of such devices should establish the desired associations and combined with a growth effort should lead to improved film quality and device performance.

### C. The effect of light power near $T_c$

We now offer an explanation for why, as  $T \rightarrow T_c$ , the light power starts to significantly perturb the system being measured.

This perturbation is seen as a spatial narrowing of  $\delta P(x)$  as  $T$  is increased while both the light power  $P_{\text{light}}$  and the microwave power  $P$  are held constant. The  $\delta P(x)$  distribution becomes significantly narrower than the physical width of the superconducting strip. Under the same conditions for which the width decreases, the shape of  $\delta P(x)$  also changes; this behavior was most noticeable in the TBCCO measurements where instead of the  $\delta P(x)$  distribution becoming flatter, the peak-to-valley ratio of  $\delta P(x)$  increased significantly (the edge photoresponse increased more rapidly than linearly with  $P_{\text{light}}$ ). Microwave power seems to be unimportant in explaining this behavior, because decreasing  $P$  did not measurably change the width or shape of the  $\delta P(x)$  distribution. The explanation cannot be specific to the mechanisms involved in the kinetic-inductance photoresponse measurement, because the same effects are observed in the resistive-transition photoresponse measurements. The absorption of light near  $T_c$  is the common feature of these two very different measurement techniques. The absorption of light itself must be altering the system being measured. This behavior is seen for both TBCCO and YBCO—one material in which  $H$  in our experiments is above  $H_{c1}$  (TBCCO) and one for which it is not (YBCO).

We believe that a reduction of  $T_c$  by several degrees near the film edges is responsible for the light-induced narrowing of  $\delta P(x)$ . As  $T$  increases, the light-induced temperature rise  $\delta T$  becomes sufficient to heat the superconductor at the film edge into the normal state—and thus contribute nothing to  $\delta P$ . Measurements of kinetic-inductance  $\delta P(x)$  performed near  $T_c$  can potentially map out  $T_c(x)$ . The faster than linear increase with light power of the kinetic-inductance  $\delta P$  that is measured near the strip edges most

likely occurs because for  $T$  near  $T_c$ ,  $\lambda(T)$  increases rapidly and it is no longer valid to assume small signal behavior (i.e.,  $\delta T \propto \delta \lambda$ ).

### D. The nature of the extrinsic photoresponse

Spatial variations in the kinetic-inductance photoresponse of the TBCCO film appear to be associated with the intergranular regions in the film. In the study of the shape of the intrinsic current distribution as a function of microwave power, these extrinsic variations were carefully removed by averaging measurements taken at many positions along the superconducting strip. The extrinsic variations, even at low  $T$  (e.g., 80 K) could be a factor of 2 in photoresponse intensity. There are two contributions that should give rise to the spikes: (1) The current is redistributed around the intergrain region over distance scales on the order of  $\lambda$ . (2) The same current flows underneath the light spot, but a small  $T$  rise enhances the magnetic field penetration more easily within the more weakly superconducting intergrain regions so a larger photoresponse is seen. At temperatures below 90 K essentially all of the extrinsic variations in the  $\delta P(x)$  measurements that we observed were increases above a  $\delta P(x)$  that resembles the intrinsic photoresponse [see Fig. 5(f)]. While a detailed explanation for the nature of all of the intergrain photoresponse spikes is not yet established, the lower temperature data suggests that enhanced flux penetration, rather than current redistribution around film imperfections is the correct explanation for the extrinsic response at lower temperatures.

## VIII. CONCLUSIONS

The dependencies of the kinetic-inductance photoresponse  $\delta P$  on the parameters on the right-hand side of Eq. (5) have been verified as follows: The measurements of  $\delta P$  while scanning the microwave frequency through the resonance yields a  $\delta P$  curve that is proportional to  $\partial P / \partial f$ . The measurement of  $\delta P$  while scanning the position of the light spot along or across the superconducting strip produces  $\delta P(x)$  curves that are proportional to  $J^2$ ; the measurements performed while scanning across the strip qualitatively match the shape predicted by a numerical calculation<sup>17</sup> for the coplanar transmission line geometry. The dependence on the total energy  $W$  stored in the resonator was verified when it was found that the quantity  $\delta P / (\partial P / \partial f) \propto (\lambda J_0)^2 / W$  remains constant independent of microwave power. The dependence  $\delta P \propto \delta \lambda$  is basic to the interpretation of the kinetic-inductance photoresponse that is presented here.

The kinetic-inductance photoresponse  $\delta P$  includes a component sensitive to the film morphology that becomes more prominent as  $T \rightarrow T_c$ . When the light spot was scanned over intergrain regions where the superconducting state was weaker, the local light-induced temperature rise caused an enhanced penetration of the magnetic field and thus a larger  $\delta P$ . The spatial profiles of  $\delta P$  were much more regular for YBCO than for TBCCO. The  $\sim 5 \mu\text{m}$  size of the  $\delta P$  variations in the TBCCO sample 1 matches the grain size in the TBCCO film. The grain size for the YBCO film was much smaller than the spatial resolution of our measurements. The

$\delta P$  spatial variations in the TBCCO sample 1 were more pronounced at higher  $T$  where the superconductivity in the intergrain regions is weaker.

For the YBCO films the following observations are consistent with no spatial redistribution of the current taking place. No change in the shape of the spatial profile  $\delta P(x)$  of the kinetic-inductance photoresponse was seen with increasing microwave power. The magnitude of  $\delta P$  scales with the microwave power as expected if there is no significant current redistribution. Over the same range of microwave powers where the kinetic-inductance photoresponse behaves like no current redistribution is occurring, the microwave power in the third harmonic increases as the cube of the applied microwave power.

For the TBCCO film no change in the intrinsic shape of the spatial profile  $\delta P(x)$  of the kinetic-inductance photoresponse was seen with increasing microwave power. The extrinsic (intergrain-associated) photoresponse was averaged out to obtain the intrinsic photoresponse. The intergrain photoresponse for the TBCCO film was much more pronounced than for the YBCO film. Over the same range of microwave powers for which no change was observed in the intrinsic shape of  $\delta P(x)$ , the rate at which the generation of power in the third harmonic  $P_3$  of the applied power  $P_1$  was significantly below the  $P_3 \propto P_1^3$  behavior observed for YBCO. These observations suggest that the generation of third-harmonic power may well be associated with intergrain regions.

## ACKNOWLEDGMENTS

We gratefully acknowledge the support of DARPA and the Office of Naval Research. This work was supported in part by Technology Reinvestment Program NASA Cooperative Agreement NCC 3-344.

<sup>1</sup>D. E. Oates, P. P. Nguyen, G. Dresselhaus, M. S. Dresselhaus, C. W. Lam, and S. M. Ali, *J. Supercond.* **5**, 361 (1992).

<sup>2</sup>A. M. Portis, *J. Supercond.* **5**, 319 (1992).

<sup>3</sup>John R. Clem and Mark W. Coffey, *J. Supercond.* **5**, 313 (1992).

<sup>4</sup>S. Sridhar, *Appl. Phys. Lett.* **65**, 1054 (1994).

<sup>5</sup>C. Wilker, Z.-Y. Shen, P. Pang, W. L. Holstein, and D. W. Face, *IEEE Trans. Appl. Supercond.* **5**, 1665 (1995).

<sup>6</sup>H. S. Newman and J. C. Culbertson, *Microwave Opt. Technol. Lett.* **6**, 725 (1993).

<sup>7</sup>L. N. Vu, M. S. Wistrom, and D. J. Van Harlingen, *Appl. Phys. Lett.* **63**, 1693 (1993).

<sup>8</sup>R. C. Black and F. C. Wellstood, *Appl. Phys. Lett.* **66**, 99 (1995).

<sup>9</sup>J. R. Kirtley, M. B. Ketchen, K. G. Stanwiasz, J. Z. Sun, W. J. Gallagher, S. H. Blanton, and S. J. Wind, *Appl. Phys. Lett.* **66**, 1138 (1995).

<sup>10</sup>J. Mannhart, H. Hilgenkamp, B. Mayer, Ch. Gerber, J. R. Kirtley, K. A. Moler, and M. Sigrist, *Phys. Rev. Lett.* **77**, 2728 (1996).

<sup>11</sup>I. F. Voloshin, N. V. Il'in, N. M. Makarov, L. M. Fisher, and V. A. Yampol'skii, *JETP Lett.* **53**, 116 (1991).

<sup>12</sup>T. Tamegai, L. Krusin-Elbaum, L. Civale, P. Santhanam, M. J. Brady, W. T. Masselink, F. Holtzberg, and C. Field, *Phys. Rev. B* **45**, 8201 (1992).

<sup>13</sup>C. P. Vlahacos, R. C. Black, S. M. Anlage, A. Amar, and F. C. Wellstood, *Appl. Phys. Lett.* **69**, 3272 (1996).

<sup>14</sup>E. Batalla, E. G. Zwartz, L. S. Wright, S. I. Raider, and A. Gupta, *J. Appl. Phys.* **69**, 7178 (1991).

<sup>15</sup>R. F. Harrington, *Time-Harmonic Electromagnetic Fields* (McGraw-Hill, New York, 1961), p. 319.

<sup>16</sup>T. Van Duzer and C. W. Turner, *Principles of Superconducting Devices and Circuits* (Elsevier, New York, 1981), Secs. 3.06–3.09.

<sup>17</sup>Calculation kindly done by Howard Snortland of Stanford University using a program written by David M. Sheen with adaptations made by Michael Tsuk. This calculation uses an approach first taken by W. T. Weeks. The technique assumes homogeneous dielectric media and thus provides solutions to coplanar transmission lines suspended in free space. Low microwave power conditions were assumed.

<sup>18</sup>W. T. Weeks, L. L. Lu, M. F. McAllister, and A. Singh, *IBM J. Res. Dev.* **23**, 652 (1979).

<sup>19</sup>D. M. Sheen, S. M. Ali, D. E. Oates, R. S. Withers, and J. A. Kong, *IEEE Trans. Appl. Supercond.* **1**, 108 (1991).

<sup>20</sup>C. Uher and A. B. Kaiser, *Phys. Rev. B* **36**, 5680 (1987).

<sup>21</sup>M. E. Reeves, D. S. Citrin, B. G. Pazol, T. A. Friedmann, and D. M. Ginsberg, *Phys. Rev. B* **36**, 6915 (1987).

<sup>22</sup>A. J. Kent and S. Chapman, *Helv. Phys. Acta* **65**, 397 (1992).

<sup>23</sup>D. W. Face, C. Wilker, J. J. Kingston, Z.-Y. Shen, F. M. Pellicone, R. J. Small, S. P. McKenna, S. Sun, and P. J. Martin, *IEEE Trans. Appl. Supercond.* **7**, 1283 (1997).

<sup>24</sup>J. S. Horwitz, D. B. Chrissey, K. S. Grabowski, and R. E. Leuchtner, *Surf. Coat. Technol.* **51**, 290 (1992).

<sup>25</sup>W. J. DeSisto, R. L. Henry, H. S. Newman, M. S. Osofsky, and V. C. Cestone, *Appl. Phys. Lett.* **60**, 2926 (1992).

<sup>26</sup>Amnon Yariv, *Quantum Electronics*, 2nd ed. (Wiley, New York 1975), p. 113.

<sup>27</sup>J. C. Culbertson, H. S. Newman, U. Strom, J. M. Pond, D. B. Chrissey, J. S. Horwitz, and S. A. Wolf, *J. Appl. Phys.* **70**, 4995 (1991).

<sup>28</sup>C. P. Bean, *Phys. Rev. Lett.* **8**, 250 (1962).